The Effect of Surface Pressure on Snowball Earth Deglaciation

Nicholas J. Edkins

A thesis submitted in fulfilment of the requirements for the degree of Master of Science in Physics, the University of Auckland, 2016.

Abstract

A 1D radiative-convective model was built to investigate the effect of surface pressure on Snowball Earth deglaciation. This type of model was chosen because it is accurate enough to replicate both the modern climate and the extreme Snowball state, but simple enough that the consequences of a large structural change can be readily understood.

Most models of the Snowball Earth keep the surface pressure fixed at its present value of 1 bar. However, deglaciation requires a CO_2 inventory in the range 0.1–0.4 bar. This substantially increases the surface pressure, which increases the surface temperature. Therefore, it would require less CO_2 to escape a Snowball state than these models would suggest.

A previous study used the correct surface pressure of 1 bar + p_{I,CO_2}, but the warming caused by the increased pressure was attributed to pressure broadening of the CO_2 absorption lines. Here it is shown that pressure broadening is not the primary effect; instead, the increase in surface pressure allows convection to extend down to higher pressures, while the energy balance at the top of the atmosphere remains unchanged. This process, which is new to the literature, is termed 'convective deepening'.

At the deglaciation threshold of 0.25 bar, compared to an atmosphere with surface pressure fixed at 1 bar, it was found that the surface is 3 K warmer if pressure broadening is included, and 13 K warmer if both pressure broadening and convective deepening are included. Therefore, convective deepening is the major source of warming when the surface pressure increases in Snowball Earth conditions.

With 0.25 bar of CO_2, c_p decreases by 3%, while $R_{specific}$ decreases by 5%, which means the moist adiabatic lapse rate increases, causing a 2 K increase in surface temperature. This effect, while smaller than convective deepening

and pressure broadening, is not negligible.

Acknowledgement

First, I'd like to thank my family, whose support has always been unconditional and unwavering.

I would also like to thank Yizhe, Jesse, Nelly, and Ben, because it's much more fun working in an atmosphere of excitement, creativity, and general knuckle-down problem solving.

Lucy, whose ability to surprise is undiminished, made this year the best yet.

Finally, I'd like to thank my supervisor, Prof. Roger Davies, from whom I learnt that a simple model can reveal a big truth. His wealth of knowledge, encouragement, and criticism have been truly invaluable throughout this process.

Contents

List of Figures

List of Tables

Abbreviations

BDBP	Binary Data Base of Profiles
CAM	Community Atmosphere Model
CRF LW	Cloud Radiative Forcing (Longwave)
CRF SW	Cloud Radiative Forcing (Shortwave)
FAT	Fixed Anvil Temperature
FOAM	Fast Ocean Atmosphere Model
GCM	Global Climate Model
GENESIS	Global Environmental and Ecological Simulation of Interactive Systems
LMDz	Laboratoire de Météorologie Dynamique zoom
LW	Longwave
NIR	Near Infrared
OLR	Outgoing Longwave Radiation
RCM	Radiative-Convective Model
SW	Shortwave
SP-CAM	Superparameterized Community Atmosphere Model
TOA	Top Of Atmosphere

CHAPTER 1

Introduction

1.1 Motivation

The Snowball Earth theory explains a lot of geological evidence, but in order to be believable, it also requires a plausible deglaciation mechanism. Every proposed mechanism requires a large amount of CO_2. However, it is overly simplistic to add a large amount of CO_2 to a model atmosphere and assume that other variables remain unchanged. Models that are designed for present Earth conditions often make assumptions of this nature in the pursuit of speed. While complex models such as global climate models (GCMs) are excellent for looking at the details of circulation and for resolving finer detail in the 3D distribution of various quantities, they are vulnerable to missing a large, simple effect if taken outside the range for which they are validated. Here, and in a previous paper [1], I argue that such an effect plays a large role in Snowball Earth deglaciation.

1.2 Organisation

The first chapter presents geological evidence supporting low-latitude glaciation, describes the different types of Snowball proposed to explain this evidence, and outlines the results of previous deglaciation modelling studies.

The second chapter describes the model functionally. It details how the longwave (LW) and shortwave (SW) radiative transfer calculations are performed, how the heating rates are calculated, how the convective adjustment

is applied, and how clouds are treated.

The third chapter describes the process of validating the model; that is, feeding in parameters describing a known climate scenario and verifying that the model output matches our knowledge of that climate. This is done for both the present Earth and the Snowball Earth.

The fourth chapter is an in-depth investigation of the values assigned to the parameters that are used to model the Snowball Earth. The reasoning behind each choice of parameter is given, and the consequences of different choices are also explored.

The fifth chapter describes how the effect of convective deepening is actually calculated. Some different approaches are described, the best is chosen, and, finally, the size of the warming effect due to convective deepening is calculated. This is compared with the warming effect due to pressure broadening alone.

The sixth chapter describes the effect of the changing atmospheric composition on the equilibrium temperature profile.

The seventh chapter takes a wider look at the phase space of the Earth system, of which the Snowball Earth is one possible state. The effect of convective deepening on this phase space is shown to be significant.

CHAPTER 2

Literature Review

Evidence has begun to converge around a remarkable hypothesis: that twice in the Neoproterozoic era, our planet was covered with ice. This is the Snowball Earth hypothesis, and it represents one of the most extreme states of which the ocean-atmosphere system is capable. As such, it requires some difficult questions to be answered; chief among them, how did the planet exit the Snowball state?

Paleomagnetic data provides evidence for a global glaciation. The Earth's magnetic field is almost parallel to the surface at the equator and perpendicular to the surface at the magnetic poles. The magnetic field changes over time, but it is 'frozen' into a rock as it solidifies, which preserves information about the former location of that rock. Therefore, samples that show near-parallel magnetic fields and evidence of glacial activity support the idea of low-latitude glaciation, which is only possible in a state of near-global glaciation.

Evidence for large CO_2 levels in the immediate aftermath of a glaciation comes from cap carbonates. These are distinctive geological formations which require a large, sudden increase in the oceanic carbonate level. This would be the consequence of a high atmospheric inventory of CO_2 suddenly being exposed to the ocean, as would be the case following a rapid deglaciation.

The state in which the planet is completely covered in ice (barring possible small and unconnected regions of open water) is called a 'hard Snowball'. The near-complete separation of the ocean and atmosphere allows for a large CO_2 inventory to build up, which explains both the eventual deglaciation and the cap carbonates left in its wake.

However, the survival of photosynthetic life through the Neoproterozoic has led to the proposal of alternative types of Snowball. One possibility is a 'Waterbelt' state, in which the tropical ocean remains ice-free. This is an attractive possibility because it provides a clear way for life to survive through a Snowball. However, a Waterbelt is less stable than other possible states, which would make a long glaciation harder to explain.

Another possible state is the Jormungand state [2], which has a much smaller area of open ocean than the Waterbelt state. The Jormungand also displays greater hysteresis than the Waterbelt. Even though an area of ocean is exposed, the low temperature and dry conditions reduce the silicate weathering rate and allow a large CO_2 inventory to build up. The Jormungand state is therefore consistent with both the survival of life and the geological evidence for high levels of CO_2 immediately after deglaciation.

It is possible that ice did in fact cover the entire planet, but remained thin near the equator—thin enough to allow enough light through that photosynthesis was possible beneath the ice. Building on McKay's [3] original proposal, the exchanges between Pollard and Kasting [4][5] and Warren and Brandt [6] have carved out a plausible parameter space in which a thin-ice solution could lie. Pollard and Kasting ultimately conclude that the thin-ice state is, like the hard Snowball, a theoretically possible state, with further work necessary to determine which (if either) actually occurred. This is essentially the status of the Waterbelt and Jormungand states as well. However, most deglaciation studies focus on the hard Snowball, since it is the most difficult to deglaciate. In this thesis, therefore, the terms 'Snowball', 'Snowball state', and 'Snowball Earth' all refer to a hard Snowball, and no distinction is made between the Sturtian and Marinoan glaciations.

The difficulty of exiting a hard Snowball state is what halted further study after it was discovered in the late 1960s by William Sellers [7] and Mikhail Budyko [8], independently. Both authors demonstrated the possible existence of this state using energy balance models. These are simple models in which the latitudinal distribution of temperature is calculated by making assumptions about the insolation, planetary albedo, infrared opacity, and horizontal heat transfer. They found that a reduction of the solar constant from its present value by 1.5–5% results in a runaway glaciation and an ice-covered planet.

This presented a problem. A planet that was covered in ice would have an albedo of approximately 0.6 — twice as high as today's. Accounting for the reduction in the solar constant, the solar energy available would have been roughly half its present value; how, then, could the ice have melted to leave the planet in its present state? Given this difficulty, the fully glaciated states revealed by the energy balance models were not regarded as actual

states reached by the Earth system in its history.

This changed with the proposal of an exit strategy by Kirschvink [9]. He proposed that when the surface is completely frozen over, the interaction between the ocean and the atmosphere ceases. Volcanoes are presumed to continue to pour CO_2 into the atmosphere; with the oceanic sink closed, it has nowhere to go, and so may accumulate to massive levels. Eventually, the large resulting greenhouse effect suffices to melt the ice, starting at the equator. Once this process begins, runaway ice-albedo feedback is enough to ensure that the ice retreats rapidly to the poles.

Caldeira and Kasting [10] tested this theory. They used an energy balance model, which indicated that 0.29 bar of CO_2 would be required to deglaciate a Snowball Earth under Neoproterozoic insolation (6% weaker than today's). This was on the upper end of what could be expected during a reasonable Snowball duration.

There is some uncertainty over the duration of the Neoproterozoic Snowball states (the Marinoan glaciation 635 million years ago and the Sturtian glaciation 720 million years ago). Bodiselitsch et al. [11], for example, estimate the duration of the Marinoan glaciation to have been 12 million years, while Hoffman et al. [12] place the maximum duration at 30 million years. Zhang and Zindler [13] estimate that the CO_2 outgassing rate would have been approximately 0.025 bar per million years, which, for a duration of 12 million years, would result in a CO_2 inventory of around 0.3 bar at the end of the glaciation; this places Caldeira and Kasting's threshold at the high end of the likely range.

However, a problem was encountered with the move to a more advanced model. Pierrehumbert [14] modelled the Snowball Earth deglaciation process using the Fast Ocean and Atmosphere Model (FOAM), a GCM. The model was only verified for up to 0.2 bar of CO_2, but at that point it was well short of deglaciation. He estimated that even 3.2 bar would not ensure deglaciation. Since this was well above the upper limit on possible CO_2 accumulation, it was now necessary, if the Snowball Earth hypothesis was to be retained, to find additional mechanisms that could reduce the deglaciation threshold to below this limit.

The first success came when different GCMs were used to model the Snowball deglaciation [15][16]. These studies found that a much lower amount of CO_2 was required to deglaciate the Snowball. The source of the discrepancy between these GCMs and FOAM was the cloud radiative forcing. FOAM had a much lower net cloud radiative forcing than the other GCMs, as a result of the way in which it calculated the cloud water content. The other GCMs were able to achieve deglaciation for reasonable CO_2 inventories (less than 0.5 bar).

Following this, other studies examined further mechanisms affecting the deglaciation threshold. One possibility raised by Abbot and Pierrehumbert [17] was the deposition of dust onto the icy surface, which would lower the albedo and therefore aid deglaciation. With an accumulation of dust, they found that deglaciation is possible for $pCO_2 = 0.01$–0.1 bar.

Yang et al. [18] added a further layer of complexity by examining the radiative effects of O_3 on Snowball deglaciation. Since the concentration of O_2 in the atmosphere may have been as low as 1–10% of its current value, the O_3 concentration would similarly have been reduced. They determined that this would lead to an increase in the deglaciation threshold by roughly 30%.

The first study to explicitly investigate the effect of surface pressure on the deglaciation problem was performed by Hu et al. [15]. They found that the deglaciation threshold decreased by about 60% when the effects of both pressure broadening and collision-induced absorption were included.

It is important to note that the deglaciation mechanisms outlined above work in tandem to produce a plausible deglaciation scenario. In this work a new mechanism is proposed which can contribute to this picture, aiding the effort to bring the deglaciation threshold to within the limits defined by the geochemical and geological evidence.

CHAPTER 3

Model Description

The radiative-convective model used in this thesis is composed of two sections: atmospheric structure and radiation. The fact that these two sections are separable allows pressure broadening and convective deepening to be isolated. This is because the surface pressure can be increased in the atmospheric structure section while remaining fixed in the radiation section, or vice versa.

3.1 Atmospheric Structure

The atmosphere is split into 100 layers of equal pressure thickness, and the temperature is initially set to an isothermal profile. This allows the thickness (in height) of each layer to be calculated from the hypsometric equation

$$\Delta z = \frac{-R_{specific} T \Delta p}{gp} \tag{3.1}$$

where g is the acceleration due to gravity, p and T are the mean pressure and temperature of the layer, $R_{specific}$ is the specific gas constant for the layer, and Δp is the pressure thickness of the layer.

The average temperature of the layer is assumed to be the mean of the temperatures at its upper and lower boundaries. The same assumption is made for the average pressure of the layer.

The total number of molecules per unit area in the atmosphere is given

by

$$N_{total} = \frac{p_{surf} N_A}{g\overline{M}} \tag{3.2}$$

where p_{surf} is the surface pressure, N_A is Avogadro's number, and $\overline{M}$ is the mean molecular weight of the atmosphere.

Since the layers are of equal pressure thickness, the molecules are split evenly between the layers. For each layer, the molar concentration of N_2, O_2, H_2O, CO_2, and O_3 is specified. The number of molecules of each species in each layer is then obtained directly: for species i, $N_i(z) = \chi_i(z) N_{total}/100$, where $\chi_i(z)$ is the molar concentration of species i in layer z.

3.2 Defining the CO_2 Amount

The amount of CO_2 present in the Earth's atmosphere is typically given in parts per million by volume (ppmv). The global annual average value for the present Earth is about 400 ppmv, which is only a trace amount compared to N_2 and O_2. Because the amount of CO_2 is so small for the present Earth, it has very little effect on the surface pressure.

However, when modelling the deglaciation of a Snowball Earth state, the amount of CO_2 *does* have an effect on the surface pressure. Therefore, it is natural to look to express the CO_2 amount in a way that reflects this. In this thesis I use the CO_2 inventory p_{I,CO_2} as described by Pierrehumbert et al. [19].

The CO_2 inventory is the pressure that the CO_2 would exert on the surface if it was the only gas present in the atmosphere

$$p_{I,CO_2} = \frac{m_{atm,CO_2} g}{A} \tag{3.3}$$

where A is the surface area of the planet and m_{atm,CO_2} is the total mass of CO_2 in the atmosphere.

The dry air inventory can be defined in the same way, so that the total surface pressure is $p_{surf} = p_{I,air} + p_{I,CO_2}$. The air inventory is fixed at 1 bar. This ignores the contribution of water vapour to the surface pressure (which depends on temperature), but this is usually negligible compared to the other two components.

The molar concentration of CO_2, χ_{CO_2}, can be calculated from

$$\chi = \frac{\frac{p_{I,CO_2}}{m_{CO_2}}}{\frac{p_{I,CO_2}}{m_{CO_2}} + \frac{p_{I,air}}{m_{air}}} \tag{3.4}$$

where m_{CO_2} is the molecular weight of CO_2, m_{air} is the mean molecular weight of the dry air, and $p_{I,air}$ is the air inventory.

It is important to note that in this thesis, the phrase '0.4 bar of CO_2 is added' means that $p_{I,CO_2} = 0.4$, not $p_{CO_2} = 0.4$. Since $p_{CO_2} = \chi p_{surf}$, when $p_{I,CO_2} = 0.4$, $p_{CO_2} = 0.29$. The discrepancy between the two is shown in Figure 3.1. The green dashed line is along $y = x$, which shows that $p_{I,CO_2} > p_{CO_2}$.

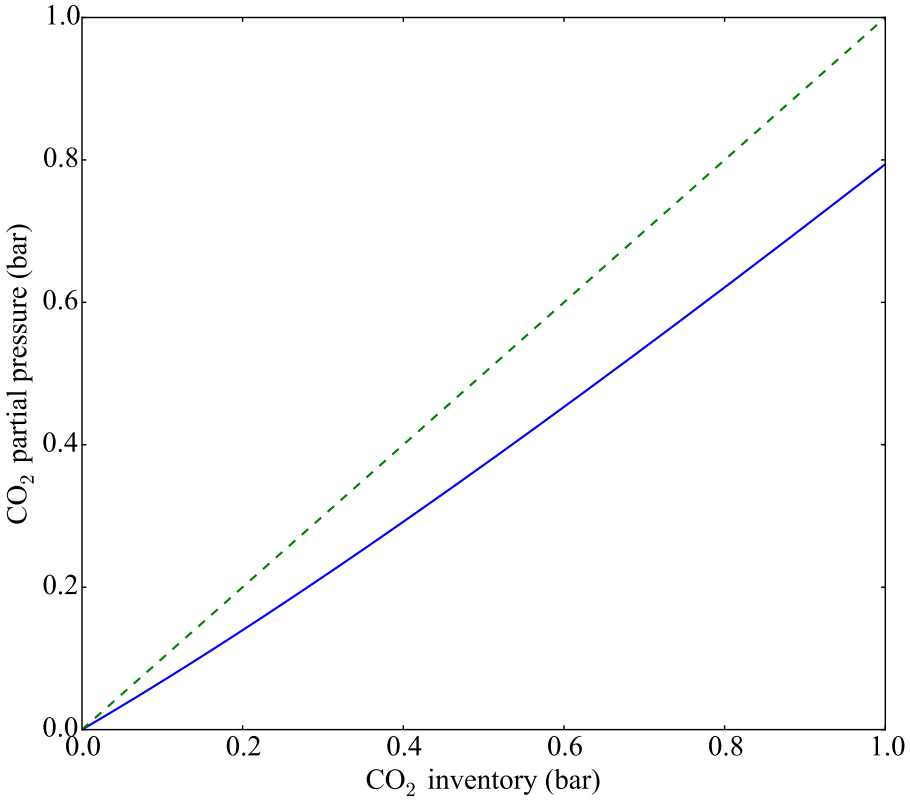

Figure 3.1: CO_2 partial pressure as a function of CO_2 inventory

With a CO_2 inventory of 0.4 bar, mistaking p_{CO_2} for p_{I,CO_2} represents an error of 27.5%, so it is important to be clear about what is meant.

3.3 Radiative Equilibrium

The main driver of the temperature structure of the atmosphere is the balance between the absorption of SW radiation and the emission of LW radiation. Therefore, the starting place for modelling is radiative equilibrium. We begin with the assumption that the horizontal variations in the radiation field and the atmosphere itself are negligible compared to the vertical variations, so that a single vertical co-ordinate (altitude or pressure) will suffice. This is the 'plane-parallel' assumption.

The fundamental equations of radiative equilibrium in a plane-parallel atmosphere are called the two-stream equations. Expressed in terms of the frequency-dependent effective optical thickness co-ordinate τ_ν, these are, for LW radiation:

$$\frac{d}{d\tau_\nu} I^\uparrow = -I^\uparrow + \pi B(\nu, T(\tau_\nu)) \tag{3.5}$$

$$\frac{d}{d\tau_\nu} I^\downarrow = I^\downarrow - \pi B(\nu, T(\tau_\nu)) \tag{3.6}$$

where $I^\uparrow$ and $I^\downarrow$ are the upward and downward fluxes, respectively, at τ_ν, $T(\tau_\nu)$ is the temperature at τ_ν, and $B(\nu, T)$ is the Planck function.

These can be solved for $I^\uparrow$ and $I^\downarrow$, which are the quantities of interest:

$$I^\uparrow(\tau_\nu, \nu) = I^\uparrow(0) e^{-\tau_\nu} + \int_0^{\tau_\nu} \pi B(\nu, T(\tau_\nu^{'})) e^{-(\tau_\nu - \tau_\nu^{'})} d\tau_\nu^{'} \tag{3.7}$$

$$I_\downarrow(\tau_\nu, \nu) = I_\downarrow(\tau_\infty) e^{-(\tau_\infty - \tau_\nu)} + \int_{\tau_\nu}^{\tau_\infty} \pi B(\nu, T(\tau_{\tau_\nu}^{'})) e^{-(\tau_\nu^{'} - \tau_\nu)} d\tau_\nu^{'} \tag{3.8}$$

where $\tau_\nu = \tau_\infty$ at the top of the atmosphere (TOA), $\tau_\nu = 0$ at the surface, and $\tau_\nu^{'}$ is a dummy variable for the integration over τ_ν. Each equation can be split into two parts: a boundary term and an atmospheric emission term.

In the first equation, the boundary term represents the upward flux from the surface, attenuated by the portion of the atmosphere between the surface and τ_ν. The second term is the sum of the emission of each layer between the surface and τ_ν, attenuated by the portion of the atmosphere that lies between that layer and τ_ν.

In the second equation, the boundary term represents the LW radiation that is incident on the TOA. We assume that only SW radiation is incident on the TOA, so this term is equal to zero. The second term is sum of the emission from each layer between the TOA and τ_ν, attenuated by the portion of the atmosphere that lies between that layer and τ_ν.

From these equations, we can calculate the difference between the energy entering and leaving a given layer. A net positive energy flow *into* a layer will

cause it to heat up, while a net flow *out of* a layer will cause it to cool down. To find the temperature change for a layer in Kelvin per day, we define the heating rate

$$H = \int_{\nu} \frac{g}{c_p} \frac{d}{dp} (I^{\uparrow} - I^{\downarrow}) \frac{seconds}{day} d\nu \tag{3.9}$$

3.3.1 The Approach to Radiative Equilibrium

Once the heating rates are obtained, they are used to perturb the temperature profile. The fluxes are then recalculated, and the temperature profile is altered again, until the conditions of radiative equilibrium are met. This process requires many iterations, each of which represents a step forward in time. At time $t + \Delta t$, the temperature of layer z is given by

$$T(z, t + \Delta t) = T(z, t) + H(z, t)\Delta t \tag{3.10}$$

The largest value of Δt that allows convergence is found through trial and error; it is between 8 and 24 hours, depending on the atmosphere in question.

3.3.2 Conditions for Radiative Equilibrium

For the atmosphere to be in radiative equilibrium, two conditions must be met:

1. At the surface, the net downward SW flux must equal the net upward LW flux. This means the lower boundary is in radiative equilibrium.

2. At the TOA, condition 1 must hold. This means the planet as a whole is in radiative equilibrium.

3.4 Longwave Radiative Transfer

The LW radiative transfer is performed using the Planetary Rapid Radiative Transfer Model (PRRTM), which is the planetary version of the Rapid Radiative Transfer Model (RRTM) [20]. PRRTM can handle pressures of up to 11 bar and large inventories of CO_2.

Section 3.3 details the analytic solutions to the equations of radiative transfer. However, the simple form of Equations 3.5 and 3.6 obscures a lot of complexity in $\tau(\nu)$, which can vary by orders of magnitude within a small wavenumber range. This makes the numerical evaluation of the integrals

in Equations 3.7 and 3.8 very time consuming, because they require a very small wavenumber step size.

PRRTM avoids this problem by using the correlated-k method.

3.4.1 The Correlated-k Method

Following Lacis and Oinas [21], the frequency distribution of absorption coefficients in a given wavenumber interval $[\nu_1, \nu_2]$ can be obtained from a given absorption spectrum by

$$f(k_i) = \frac{1}{\nu_2 - \nu_1} \sum_{j}^{M} \left| \frac{\Delta \nu_j}{\Delta k_i} \right| W(k_i, k_i + \Delta k_i) \tag{3.11}$$

where k_ν is the monochromatic absorption coefficient, M is the number of subintervals and W is a rectangular function that is zero outside the interval $[k_i, k_i + \Delta k_i]$ and unity inside. This frequency distribution is then normalised over the wavenumber interval.

The cumulative frequency distribution is then defined

$$g(k_n) = \sum_{i=1}^{n} f(k_i) \Delta k_i \tag{3.12}$$

This function is much smoother than the absorption spectrum from which it is derived, which allows for a larger stepsize when integrating. Taking the inverse of this function, $k_n(g) = g^{-1}(k_n)$, the integration can be done over g instead of over ν. The number of k intervals, n, does not need to be large in order to describe $g(k)$

To account for pressure broadening, these k distributions are created using the absorption spectra for several different pressures. There are two consequences of pressure broadening: there is a greater amount of absorption over a given wavenumber interval, and the range between the highest and lowest absorption coefficients present in the wavenumber interval decreases. Both of these also occur in $k(g)$.

It is then possible to model an increase in pressure broadening, by selecting the k distribution for a higher pressure, without increasing the surface pressure in the atmospheric structure routine. This is described in Section 6.2.

3.5 Shortwave Radiative Transfer

The SW radiative transfer is performed using Lacis and Hansen's parameterisation [22]. This requires as inputs the vertical profiles of H_2O, O_3, cloud optical depth and fraction, and the surface albedo and zenith angle. With these, the net SW flux through each level can be calculated, and from this it is simple to find the SW heating rates.

3.5.1 Ozone Absorption

Lacis and Hansen provide a parameterisation for the fraction of the incident SW radiation absorbed by O_3:

$$A_{O_3}(x) = \frac{0.02118x}{1 + 0.042x + 0.000323x^2} + \frac{1.082x}{(1 + 138.6x)^{0.805}} + \frac{0.0658x}{1 + (103.6x)^3}$$

where x is the ozone amount in cm at NTP.

This is used to calculate the net flux due to absorption by O_3 in layer l

$$F_{l,net}^{O_3} = \pi F_0 \mu_0 \{A_{O_3}(x_{l+1}) - A_{O_3}(x_l) + \bar{R}(\mu_0)[A_{O_3}(x_l^*) - A_{O_3}(x_{l+1}^*)]\}$$

where πF_0 is the solar constant, μ_0 is the cosine of the zenith angle, x_l is the ozone amount encountered by a beam of solar radiation travelling from the TOA to the l^{th} layer, x_l^* is the ozone amount encountered by a beam incident on the l^{th} layer from below, accounting for the slant path and for refraction, and $\bar{R}(\mu_0)$ is the effective albedo of the 'reflecting region', which includes the surface and the lower atmosphere.

This net flux can be combined with the net flux due to SW H_2O absorption to obtain the total heating rates due to SW absorption.

3.5.2 Water Vapour Absorption

Multiple scattering from clouds plays a large role in the SW absorption of water vapour, so the parameterisation is divided into a clear sky section and a cloudy sky section.

Clear Sky

Lacis and Hansen also provide a similar parameterisation to calculate the fraction of the incident SW radiation absorbed by H_2O:

$$A_{H_2O}(y) = \frac{2.9y}{(1 + 141.5y)^{0.635} + 5.925y}$$

where y is the water vapour amount in cm.

For a clear sky, the net flux can be calculated in the same way as for O_3

$$F_{l,net}^{H_2O,clear} = \mu_0 \pi F_0 \{A_{H_2O}(y_{l+1}) - A_{H_2O}(y_l) + R_g[A_{H_2O}(y_l^*) - A_{H_2O}(y_{l+1}^*)]\}$$

where R_g is the surface albedo. The effective water vapour amount for a solar beam starting from the TOA and reaching the l^{th} layer is defined as

$$y_l = \frac{M}{g} \int_0^{p_l} q \left(\frac{p}{p_0}\right) \left(\frac{T_0}{T}\right)^{\frac{1}{2}} dp$$

where M is the magnification factor, q is the specific humidity, and g is the acceleration due to gravity, while the effective water vapour amount reaching the l^{th} layer from below is

$$y_l^* = \frac{M}{g} \int_0^{p_{surf}} q \left(\frac{p}{p_0}\right) \left(\frac{T_0}{T}\right)^{\frac{1}{2}} dp + \frac{5}{3g} \int_{p_{l+1}}^{p_{surf}} q \left(\frac{p}{p_0}\right) \left(\frac{T_0}{T}\right)^{\frac{1}{2}} dp$$

The pressure and temperature scaling distinguish the water vapour absorption from the simpler ozone absorption.

Cloudy Sky

Table 3.1 shows the probability distribution that is used to calculate the absorption for cloudy skies; $p(k)dk$ is the fraction of the incident solar flux that encounters an absorption coefficient in the range k to $k + dk$.

n	k_n	$p(k_n)$
1	0.00004	0.6470
2	0.002	0.0698
3	0.035	0.1443
4	0.377	0.0584
5	1.95	0.0335
6	9.4	0.0225
7	44.6	0.0158
8	190	0.0087

Table 3.1: Probability distribution of water vapour absorption coefficients from Lacis and Hansen [22]

To calculate the reflection and transmission functions for each layer due to both cloud and water vapour, Lacis and Hansen define

$$u = \left(\frac{1 - g\tilde{\omega}_{l,n}}{1 - \tilde{\omega}_{l,n}} \right)^{\frac{1}{2}} \tag{3.13}$$

$$t = [3(1 - \tilde{\omega}_{l,n})(1 - g\tilde{\omega}_{l,n})]^{\frac{1}{2}} \, \tau_{l,n} \tag{3.14}$$

where $\tilde{\omega}_{l,n}$ is the single scattering albedo for the l^{th} layer, $\tau_{l,n}$ is the total optical depth for the l^{th} layer (both cloud and water vapour), and g is the asymmetry factor, which is 0.85 here. The probability distribution is divided into several bands, and the subscript n refers to these bands.

The reflection and transmission functions for a cloud layer then follow

$$R_l = R_l^* = \frac{(u+1)(u-1)(e^t - e^{-t})}{(u+1)^2 e^t - (u-1)^2 e^{-t}} \tag{3.15}$$

$$T_l = T_l^* = \frac{4u}{(u+1)^2 e^t - (u-1)^2 e^{-t}} \tag{3.16}$$

where R_l^* and T_l^* are the reflection and transmission functions for illumintation from below.

The reflection and transmission functions for a clear layer are simpler

$$R_l = R_l^* = 0 \tag{3.17}$$

$$T_l = T_l^* = exp(-5\tau_{l,n}) \tag{3.18}$$

The next step is to calculate the reflection and transmission functions for a composite layer made up of two layers a and b.

$$R_{ab} = R_a + \frac{T_a R_b T_a^*}{1 - R_a^* R_b} \tag{3.19}$$

$$T_{ab} = \frac{T_a T_b}{1 - R_a^* R_b} \tag{3.20}$$

$$R_{ab}^* = R_b^* + \frac{T_b^* R_a^* T_b}{1 - R_a^* R_b} \tag{3.21}$$

$$T_{ab}^* = \frac{T_b^* T_a^*}{1 - R_a^* R_b} \tag{3.22}$$

Once a process for doing this is established, it can be repeated iteratively to find the upward and downward fluxes at each layer boundary

$$U_l = \frac{T_{1,l} R_{l+1,L+1}}{1 - R_{1,l}^* R_{l+1,L+1}} \tag{3.23}$$

$$D_l = \frac{T_{1,l}}{1 - R_{1,l}^* R_{l+1,L+1}} \tag{3.24}$$

From this, it is simple to calculate the net flux through each layer due to H_2O absorption. For a given layer l, the atmosphere can be divided into the composite layer above l, from layer 1 to l, and the one below it, from $l+1$ to $L+1$, where L is the total number of atmospheric layers. The fraction of the incident solar beam absorbed in the upper composite layer is

$$A_{1,l}(n) = p(k_n)[1 - R_{1,L+1}(n) + U_l(n) - D_l(n)] \tag{3.25}$$

which means the net flux through layer l is

$$F_{l,net}^{H_2O,cloudy}(n) = \pi F_0(A_{l-1,l}(n) - A_{l-1}(n)) \tag{3.26}$$

3.5.3 Column Model

The method of calculation of the SW flux profile for a totally clear atmosphere or an atmosphere with a single cloud has been established. However, to model the atmosphere realistically, it is necessary to include multiple cloud layers, which may overlap each other. Therefore, the atmosphere is divided into three cloudy columns, each of which contains a single cloud layer, and one clear column. The vertical flux profile is computed for each column, and then the fluxes for each column are weighted and added to give the total average vertical SW flux profile, from which the SW heating rates can be calculated.

In order to weight the fluxes, an assumption must be made about the way the clouds overlap. I assume random cloud overlapping, so that two cloud layers with fractions f_a and f_b have an overlapped fraction $f_{ab} = f_a \times f_b$. The cloudy fraction for these two layers combined is then $f_a + f_b - f_{ab}$, which means that the clear sky fraction for these two layers is $1 - (f_a + f_b - f_{ab})$. This process can be repeated in an iterative way, taking f_a now as the cloudy fraction of the composite layer made up of the initial two layers, and f_b as the cloudy fraction of a new, third layer.

Once every cloud has been included, the total clear sky fraction can be calculated. The net flux profile for the clear column is multiplied by this fraction. To this, I add the flux profile of each cloudy column, weighted by the cloud fraction of that layer multiplied by the total cloudy fraction (i.e. $1 - f_{clear,total}$).

3.6 Heating Rates

Once both SW and LW fluxes have been obtained as described above, they can be used to calculate the heating rate for each layer. The heating rate of

a layer in units of Kelvin per day is given by

$$\frac{\Delta T}{\Delta t} = \frac{g}{c_p}\frac{\Delta F_{net}}{\Delta p}\frac{seconds}{day} \tag{3.27}$$

where $F_{net} = F_{net}^{O_3} + F_{net}^{H_2O,clear} + F_{net}^{H_2O,cloudy} + F_{net,LW}$.

For each timestep, the heating rates are calculated and added to the temperature profile. The altitude of each layer is then recalculated using Equation 3.1. The radiative transfer routines are called again, and the heating rates recalculated, until the equilibrium conditions are met (see Section 3.9).

Equation 3.27 contains c_p, which is dependent on the atmospheric composition, so it is important to calculate c_p properly when the CO_2 inventory is changed.

3.7 Convective Adjustment

The method of applying the convective adjustment follows Manabe and Strickler [23]. Whenever, in the course of running the model, the lapse rate between two layers exceeds the critical lapse rate, it is adjusted down to the critical lapse rate:

$$\text{if } \frac{\Delta T}{\Delta z} > -\Gamma_{critical} \text{ then } \Delta T = -\Gamma_{critical}\Delta z$$

The justification for this approach is that the convective relaxation time is much shorter than the radiative relaxation time. We are only interested in the radiative-convective equilibrium, not the approach to that state, so we can treat convection as occuring instantaneously.

The choice of the value of the critical lapse rate for the Snowball Earth is discussed in Chapter 5, and effect of the changing atmospheric composition on the lapse rate is discussed in Chapter 7.

3.8 Clouds

The clouds in the model are grey. Each of the 100 atmospheric layers can be assigned a cloud fraction and a cloud optical depth. This allows for a detailed cloud profile to be fed into the model. However, for the purposes of this study, a detailed cloud profile is not required. When replicating the present Earth's climate, the aim is to show that reasonable parameters give a reasonable approximation of the observed climate. When modelling the

Snowball Earth, the limiting factor on the accuracy is our lack of knowledge about cloud conditions in that state, not the level of detail of the model. Therefore, three cloud layers are used in this study. Their heights, fractions, and optical depths are the parameters that can be controlled.

3.9 Conditions for Radiative-Convective Equilibrium

The requirements for the atmosphere to be in radiative-convective equilibrium are

1. At the TOA, the outgoing LW radiation (OLR) must equal the total absorbed SW radiation. This ensures that the atmosphere as a whole is in equilibrium.

2. The surface radiation budget (the downward flux minus the upward flux) must be equal to the net integrated radiative cooling of the atmosphere.

3. In a layer where convection does not occur, the usual conditions of radiative equilibrium must be satisfied.

CHAPTER 4

Validation of the Model

In order for the results of the model to be trusted, it should be able to match observations when they are available. When they are not available, it should be able to replicate the results of other models when fed the same parameters.

In the first section of this chapter, the climate of the present Earth is replicated. This confirms that no major sacrifices were made when adapting the model for extreme, high-CO_2 conditions. In the second section, the model is given the same parameters as a previous radiative-convective model of the Snowball Earth [15], and produces similar output. This confirms that the model also works as expected in Snowball Earth conditions.

4.1 Present Earth

The following describes how the choices for the value of each parameter were made for the present Earth. The resultant temperature profile is shown to agree well with the observed profile.

4.1.1 Clouds

The planetary albedo is the proportion of the incoming radiation from the Sun that is reflected by the Earth. It is the most important parameter to determine, because the amount of reflected radiation at the TOA directly determines the amount of energy available to heat the atmosphere. Satellites have measured the Earth's planetary albedo to be 0.29 [24].

In this model, the planetary albedo can only be changed indirectly by changing the surface albedo and the cloud properties. With a surface albedo of 0.17 and clouds following Manabe and Wetherald [25], a planetary albedo of 0.29 is obtained.

Cloud	Cloud Top Height (km)	Fraction	Optical Depth
High	10.0	0.228	1.0
Mid	4.1	0.090	20.0
Low	2.7	0.313	20.0

Table 4.1: Cloud properties for present Earth

For a planetary albedo of 0.29, the total absorbed SW radiation is

$$\frac{1362}{4} \times (1 - 0.29) = 242\,\mathrm{W\,m^{-2}}$$

The other important quantity that clouds affect is the OLR. If the model is to replicate the climate of the present Earth, the cloud profile should give an OLR of $242\,\mathrm{W\,m^{-2}}$ when the surface temperature is at the current observed value of 288 K [26]. The profile in Table 4.1 also satisfies this condition.

4.1.2 Gas Mixing Ratios

CO_2 is a well-mixed gas, so the vertical profile is constant. A value of 400 ppmv was chosen.

H_2O and O_3 are more complicated. The common method for H_2O is to assume that the relative humidity remains fixed according to some constant profile, which allows the specific humidity to increase as temperature increases. Here, the profile chosen is from Manabe and Wetherald [25]:

$$h = h_* \left(\frac{Q - 0.02}{1 - 0.02} \right) \tag{4.1}$$

where h_* is the relative humidity at the surface, set to 0.77, and $Q = p/p_{surf}$. The relative humidity becomes negative if $Q < 0.02$, so if the H_2O mixing ratio obtained from Equation 4.1 falls below a minimum value of 3 ppmv, it is reset to this value.

The vertical distribution of O_3 is obtained using the Binary Data Base of Profiles (BDBP) [27]. By averaging over latitude and over the years 1979–2006, the global annual average O_3 vertical profile is obtained, as shown in Figure 4.1.

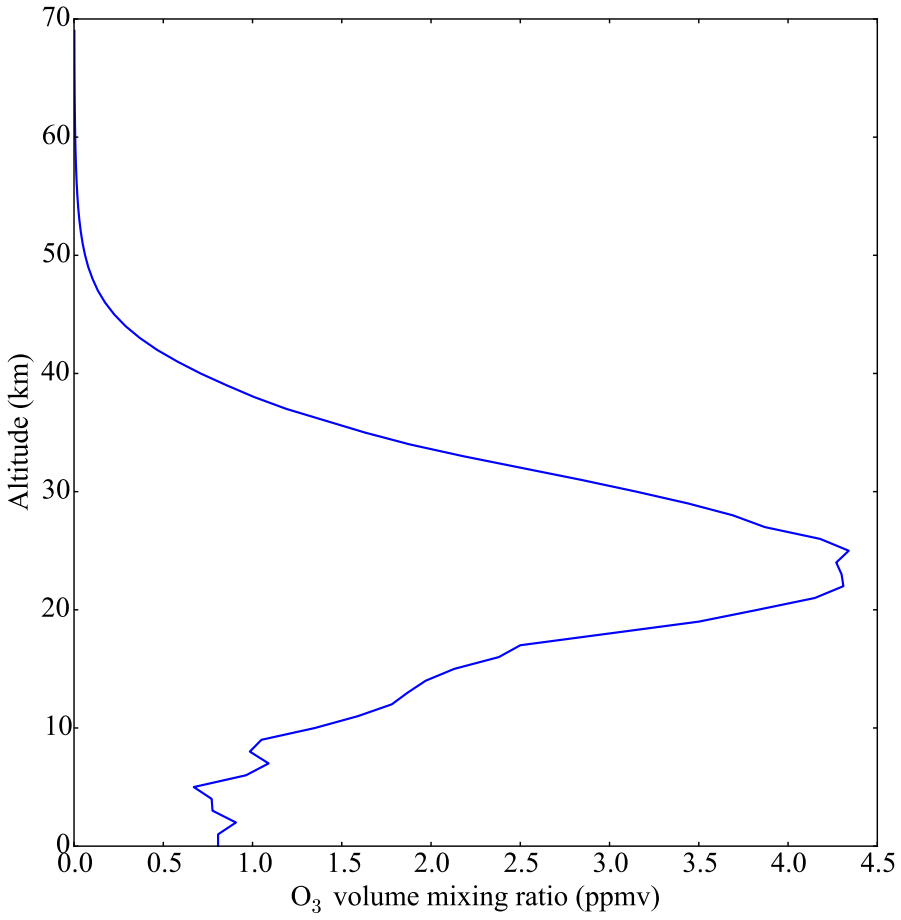

Figure 4.1: Global annual average O_3 mixing ratio for the years 1979–2006 obtained from the BDBP database

4.1.3 Lapse Rate

Most radiative-convective models of the present Earth use either the moist adiabatic lapse rate or a value of $\Gamma = 6.5\,\mathrm{K\,km^{-1}}$ for the critical lapse rate. However, since the aim is to replicate the observed climate, it is appropriate to use the observed global average lapse rate of $5.7\,\mathrm{K\,km^{-1}}$ [28].

4.1.4 Agreement with Observations

The radiative-convective equilibrium temperature profile with the above parameters is shown in Figure 4.2. It shows a slight stratospheric temperature inversion, as does the observed global average temperature profile. The tropopause is at 220 K, which agrees well with the tropopause temperature of the US Standard Atmosphere [29], which is 217 K. Most importantly, the surface temperature is 288 K, which agrees closely with the observed result. This confirms that the model is capable of replicating the present climate of the Earth.

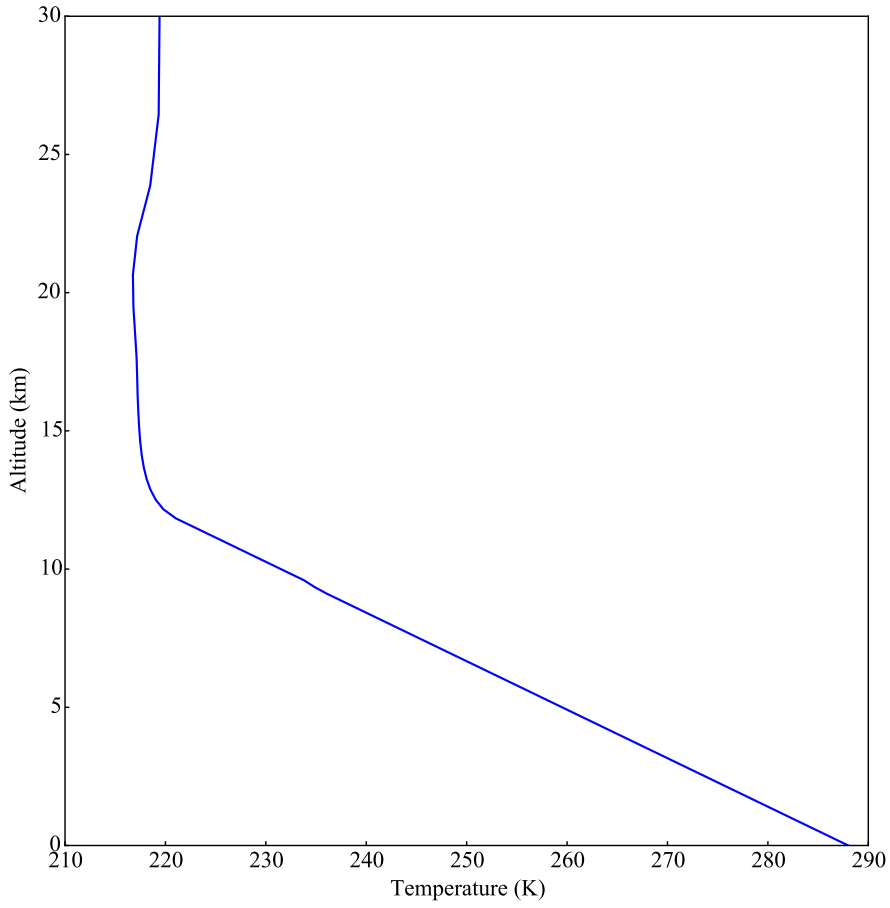

Figure 4.2: Radiative-convective equilibrium temperature profile for present Earth conditions

4.2 Snowball Earth

The agreement of the model with observations confirms that it works in the parameter space associated with present Earth. However, in order to test the model in a Snowball Earth parameter space, which is characterised primarily by low temperatures and very high CO_2 inventories, there are no observations with which to compare it. Therefore, the best comparison that can be made is with other modelling studies.

The best candidate for a comparison is the study by Hu et al. [15]. This study is one of the few to use a radiative-convective equilibrium model to examine Snowball Earth deglaciation. The authors also point out the surface pressure increase that results from a large CO_2 inventory.

In this section, I choose parameters to best replicate their study. In the following chapter, the best estimate for each parameter is examined in detail, which results in some differences.

4.2.1 Planetary Albedo

Hu et al. use a surface albedo of 0.663. Caldeira and Kasting [10], from whose paper Hu et al. take this number, state that a surface albedo of 0.663 results in a planetary albedo of 0.62 in modern polar conditions. As described below, Hu et al. don't include clouds in their model, so I set the surface albedo to 0.663 but use the planetary albedo of 0.62 when determining the total absorbed SW radiation.

4.2.2 Clouds

Hu et al., using Kasting's model, do not include clouds explicitly. Instead, they find the OLR with a clear sky. They then assume that the LW cloud forcing is equal to $15.66\,\mathrm{W\,m^{-2}}$, and subtract this value from the OLR. This number is fairly representative of the LW cloud forcings found using GCMs at high CO_2 inventories. However, the fact that it is fixed means that no cloud feedback is possible. In this chapter, I use the same constant reduction to the OLR; in Chapter 5, I describe how to model clouds in the Snowball Earth in more detail.

4.2.3 Gas Mixing Ratios

As usual, the CO_2 is well-mixed. For the H_2O distribution, Hu et al. follow Manabe and Wetherald's profile as in Equation 4.1, but with a surface relative humidity of 80%.

4.2.4 Lapse Rate

Hu et al. do not state the value used for the critical lapse rate in their radiative-convective model. Since the dry and moist adiabatic lapse rates are very similar in Snowball conditions [30], I use the dry adiabatic lapse rate to replicate Hu et al.'s study. This is given by

$$T(p) = T(p_{surf}) \left(\frac{p}{p_{surf}} \right)^{\frac{R}{c_p}} \tag{4.2}$$

4.2.5 Agreement with Previous Study

With the parameters set the same way as in the study of Hu et al., the equilibrium surface temperature for various CO_2 mixing ratios is found. A comparison with the results of Hu et al. is made in Figure 4.3.

In order for the planet to deglaciate, the annual mean temperature *at the equator* must be slightly above 273 K. Once the equatorial ice begins to melt, ice-albedo feedback acts to ensure that the rest of the ice melts. Hu et al. [15] found that in a Snowball state the global annual mean temperature is around 10 K lower than the equatorial annual mean temperature. Therefore, a global annual mean temperature of 263 K is sufficient to ensure deglaciation.

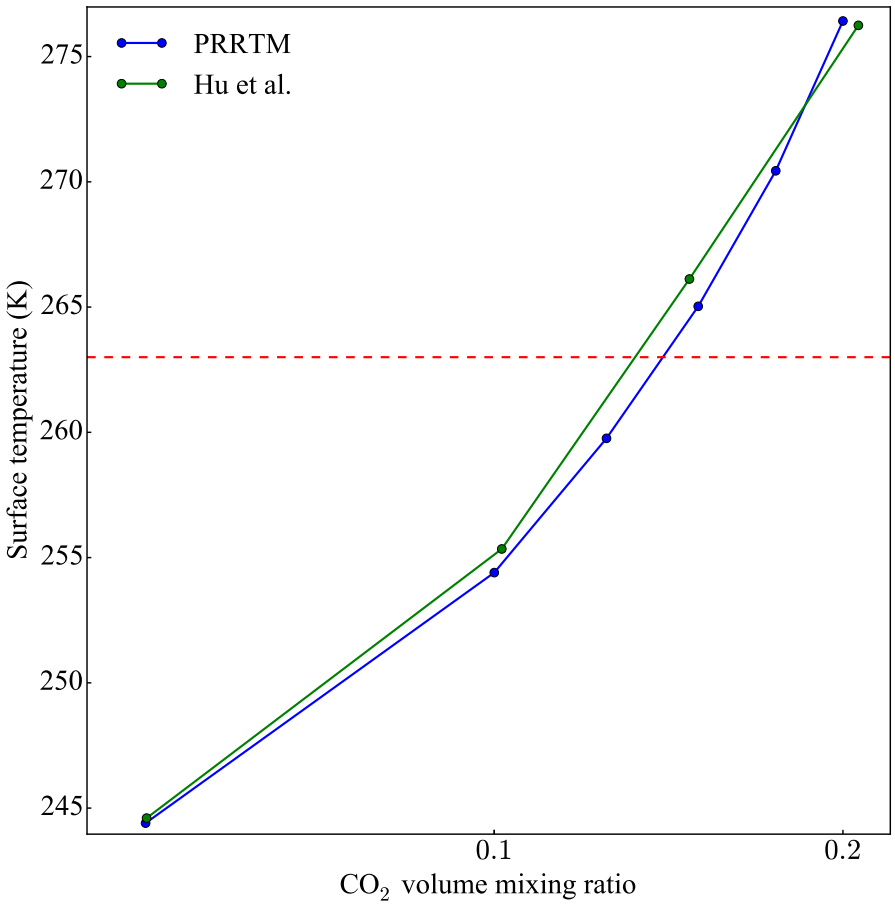

Figure 4.3: Comparison between Hu et al. and PRRTM. The dashed red line is at 263 K, where deglaciation occurs.

It is clear that the two models produce very similar outputs when given the same parameters. Hu et al. found a deglaciation threshold of 0.21 bar; the value in my model is 0.25 bar. The close agreement between the models suggests that my model is capable of simulating the Snowball Earth climate.

CHAPTER 5

Best Choices for Snowball Parameters

In this chapter, I investigate the different possible choices for some parameters during a Snowball Earth. I test the effect of different assumptions about the parameters to get an idea of the importance of the assumption. I then make a decision as to the best value for each parameter, and these are the values that are used through the rest of the study.

5.1 Water Vapour

For the colder temperatures of the Snowball Earth, all modellers agree that the absolute humidity will be lower than it is on the present Earth. However, an assumption has to be made about the relative humidity profile. Some studies use a constant vertical profile in the troposphere [19], while others [15] use Manabe and Wetherald's [25] profile (see Equation 4.1).

There is some evidence that a constant vertical relative humidity, rather than Manabe and Wetherald's profile, which decreases with pressure, is more typical in cold conditions. Tomasi et al. [31] observed a fairly constant relative humidity profile in Antarctica.

GCM results add even more complexity to this picture. Pierrehumbert [32] notes that, due to the low thermal inertia of the surface, there is a strong diurnal temperature cycle. This results in a low relative humidity in the boundary layer, which can lead to relative humidity *increasing* with height. This is also seen in Figure 3a in Hu et al. [15]. The different relative humidity profiles used in Snowball modelling, as well as the observed average

profile in Antarctica, are shown in Figure 5.1.

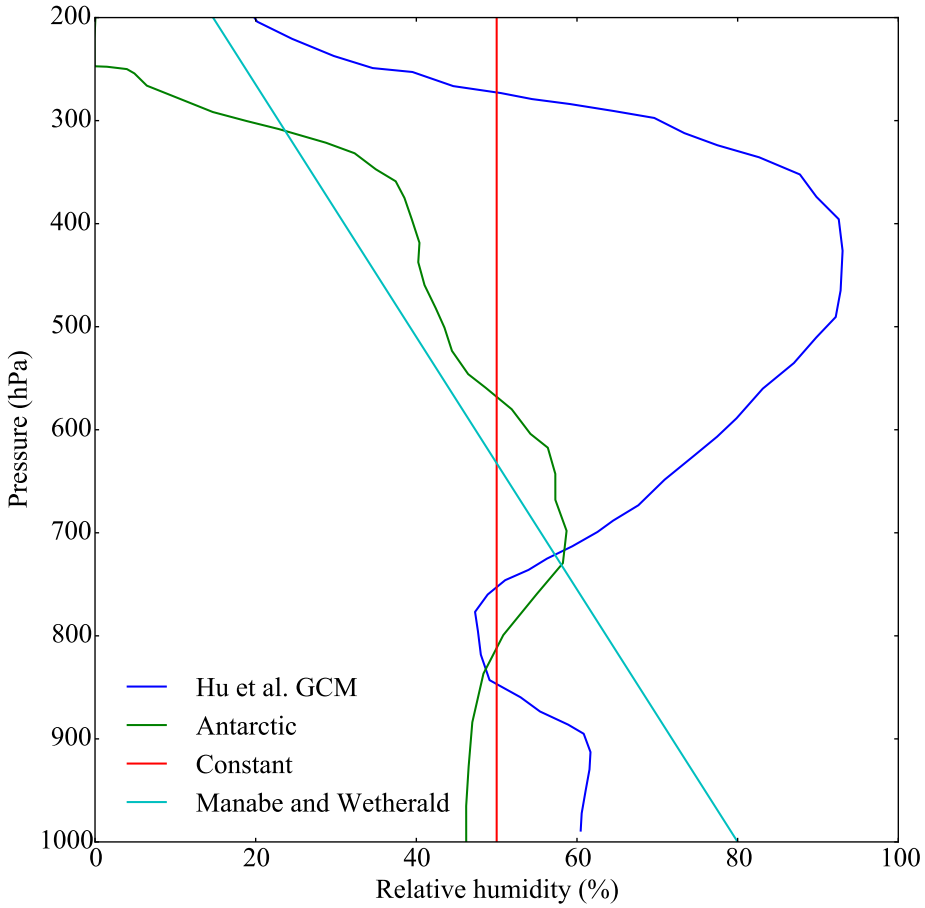

Figure 5.1: Various relative humidity profiles relevant to Snowball Earth modelling

Manabe and Wetherald's profile stays fairly close to the average of the other profiles, and it displays the decrease of relative humidity with height in the upper troposphere seen in Hu et al. and Tomasi's profiles. It also has the advantages of being in common use and of being a simple analytic formula. Therefore, in this study, the relative humidity follows Manabe and Wetherald's profile. However, a case could be made for a similar profile, but with constant relative humidity for pressures greater than 700 hPa, to account for Pierrehumbert's argument and Hu et al.'s results.

The model was run with both Manabe and Wetherald's profile and a constant profile with 50% relative humidity in order to determine the size of the effect that the choice of relative humidity profile has on the surface temperature. Figure 5.2 shows that, while the stratospheric temperature can vary by roughly 5 K, the surface temperature only varies by 0.2 K. Therefore, while an effort is made to use a suitable relative humidity profile, a different choice would not significantly impact the results presented in this thesis.

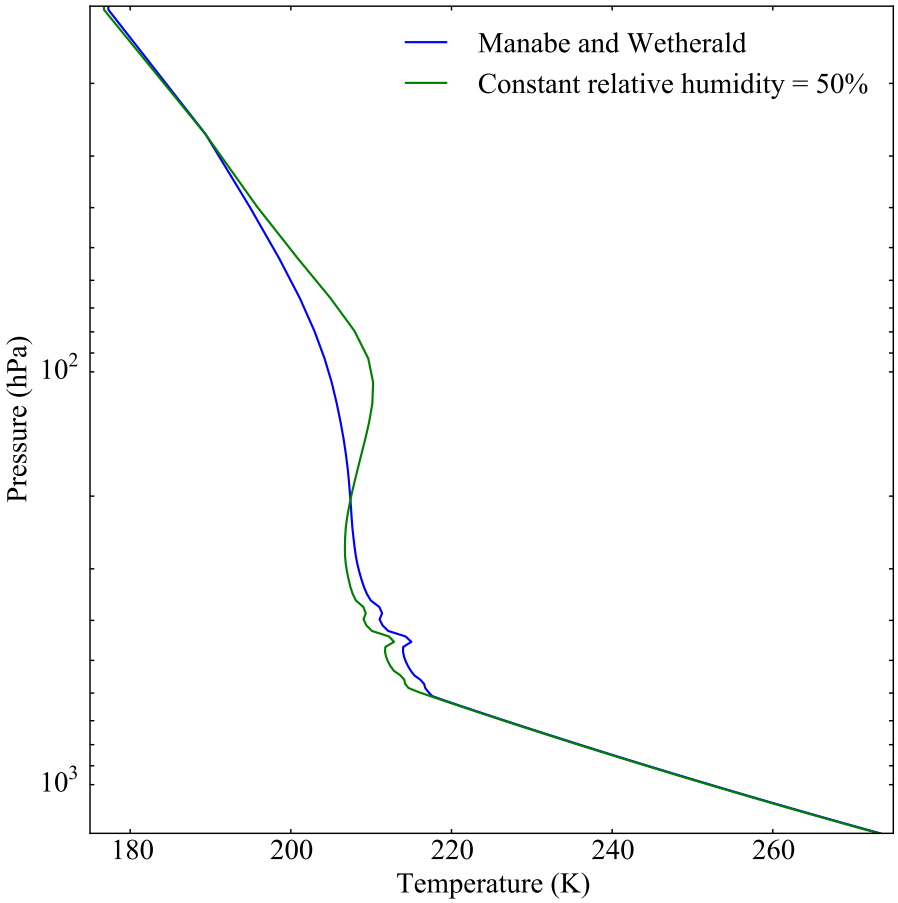

Figure 5.2: The equilibrium temperature profiles for two different relative humidity profiles

5.2 Lapse Rate

Abbot found that the temperature profile in a Snowball Earth closely followed the moist adiabat. This is given by

$$\Gamma_m = \frac{g}{c_p} \frac{\left(1 + \frac{L\mu_s}{R_a T}\right)}{\left(1 + \frac{L^2 \mu_s}{c_p R_v T^2}\right)} \tag{5.1}$$

where L is the latent heat of condensation per unit mass of H_2O, μ_s is the saturation mixing ratio of H_2O, R_a is the specific gas constant of dry air, and R_v is the specific gas constant of water vapour.

This is the critical lapse rate used in the rest of this study.

However, Abbot also found that for a Snowball Earth the release of latent heat by condensation did not significantly decrease the lapse rate, unlike the case of the present Earth. This means that, while the lapse rate is very close to the dry adiabatic lapse rate, clouds do in fact form. He also states that it does not require much cloud ice to form a cloud that is optically thick in the LW region.

5.3 Clouds

Clouds are crucially important to the deglaciation problem. The first GCM studies of the Snowball Earth deglaciation using FOAM showed a very high deglaciation threshold, but they also had very small values of cloud radiative forcing. This was a result of the simple cloud scheme in FOAM. When different GCMs were trained on the problem, they produced cloud radiative forcings of 15–20 $\mathrm{W\,m^{-2}}$, which significantly aided in deglaciation.

Abbot [30] then studied Snowball Earth clouds using a cloud-resolving model. The picture of Snowball clouds that he presented was of relatively low, optically thick ice clouds. He also found a cloud radiative forcing of 10–20 $\mathrm{W\,m^{-2}}$. Another key finding was that when the cloud ice profiles were normalised and plotted against temperature, they followed the same curve. This is confirmation of the fixed anvil temperature (FAT) hypothesis, which states that the top of the highest cloud remains at a constant temperature under climate perturbations, due to the radiative cooling of water vapour [33].

Taking all of this information into account, it is clear that the clouds in the model should have certain properties:

1. They should have a net cloud radiative forcing of roughly 15 $\mathrm{W\,m^{-2}}$

Paper	Year	CRF	CRF LW	CRF SW	Fraction	Height	Pressure	Temperature
Abbot [30]	2014	18.0	23.0	-5.0			900	200–240
Abbot et al. [16] FOAM	2012	2.0					950	
Abbot et al. [16] LMDz	2012	15.0					900-500	
Abbot et al. [16] CAM	2012	10.0					1000-600	
Abbot et al. [16] SP-CAM	2012	17.0					1000-450	
Abbot et al. [16] GENESIS	2012	40.0					950-850	
Abbot et al. [17]	2010		15.0					
Le Hir et al. [34]	2010	6.5	13.6	-7.1				
Pierrehumbert [32]	2005	2.5	10.5		'near total'	0–1.4		

Table 5.1: Cloud properties in previous Snowball modelling studies. Height, temperature and pressure refer to the peak of the distribution. The pressure range represents the pressures for which the cloud condensate is greater than $5\,\mathrm{mg\,m^{-3}}$. The values from Abbot et al. [16] are for the case where the CO_2 mixing ratio is 0.1. Abbreviations: Laboratoire de Météorologie Dynamique zoom (LMDz), Community Atmosphere Model (CAM), Superparameterized Community Atmosphere Model (SP-CAM), Global Environmental and Ecological Simulation of Interactive Systems (GENESIS), Cloud Radiative Forcing (CRF).

2. They should be optically thick in the LW region

3. They should occur mostly in the temperature range 240–200 K

5.4 Surface Albedo

Surface albedo is the single most important factor in Snowball Earth deglaciation. An increase of only 5% can decrease the total absorbed SW radiation by more than $5\,\mathrm{W\,m^{-2}}$, which requires a significant increase in CO_2 inventory to compensate. However, many modellers do not clearly report the exact value of surface albedo, which can make comparison between studies difficult. Table 5.4 summarises the information about the albedo given in recent modelling studies of the Snowball Earth deglaciation.

Abbot uses a surface albedo of 0.6 in his recent studies, assuming some regions of dusty ice. Since this thesis neglects the effect of dust on deglaciation, the surface will be covered mostly with sea ice ($\alpha \approx 0.6$) with some snow ($\alpha \approx 0.75$), so a slightly higher albedo is appropriate.

Hu et al. use 0.663, but this value is carried over from Caldeira and Kasting's earlier model [10]. Therefore, the most recent, appropriate value of surface albedo for a dust-free Snowball state is 0.64 from Le Hir et al. This is used throughout the rest of this thesis.

Paper	Year	Surface	Snow	Ice	Planetary
Abbot [30]	2014	0.600			
Abbot et al. [16]	2012	0.600			
Yang et al. [18]	2012	0.780	0.50		
Pierrehumbert et al. [19]	2011			0.55-0.65	
Hu et al. [15] GCM	2011	visible: 0.900	0.50		
		NIR: 0.600			
Hu et al. [15] RCM	2011	0.663			0.62
Abbot et al. [17]	2010		0.79	glacial: 0.65	
				sea: 0.45	
Le Hir et al. [35]	2010			visible: 0.65	FOAM: 0.65
				NIR: 0.45	LMDz: 0.60
Le Hir et al. [36]	2007	0.640		land: 0.77	
				sea: 0.60	
Lewis et al. [37]	2006		control: 0.65	0.50	
Pierrehumbert [32]	2005		0.75	0.50	
Pierrehumbert [14]	2004		0.75	0.50	
Crowley et al. [38]	2001			0.45	

Table 5.2: Surface and planetary albedos in previous Snowball modelling studies. Abbreviations: Radiative-convective Model (RCM), Near Infrared (NIR).

CHAPTER 6

Testing Convective Deepening

In this chapter, some different solutions to the problem of how to compare an atmosphere with a fixed surface pressure to one with a correctly varying surface pressure are discussed. This is important because the surface temperature increases when the surface pressure increases. I aim to calculate how much of this surface temperature increase is due to non-radiative consequences of increasing the surface pressure (i.e., to convective deepening rather than pressure broadening).

In order to do this, I first produce an equilibrium temperature profile with the correct surface pressure. The CO_2 inventory is 0.4 bar, and the surface pressure is 1 bar + p_{I,CO_2}, which is 1.4 bar. The critical lapse rate is the moist adiabat. The surface albedo is set to 0.66. The model is run to radiative-convective equilibrium, and the equilibrium surface temperature is 263 K, which means that the planet is at the point of deglaciation with 0.4 bar of CO_2. The OLR and the absorbed SW are both equal to 121.5 Wm^{-2}. The temperature profile and CO_2 distribution are shown in Figure 6.1.

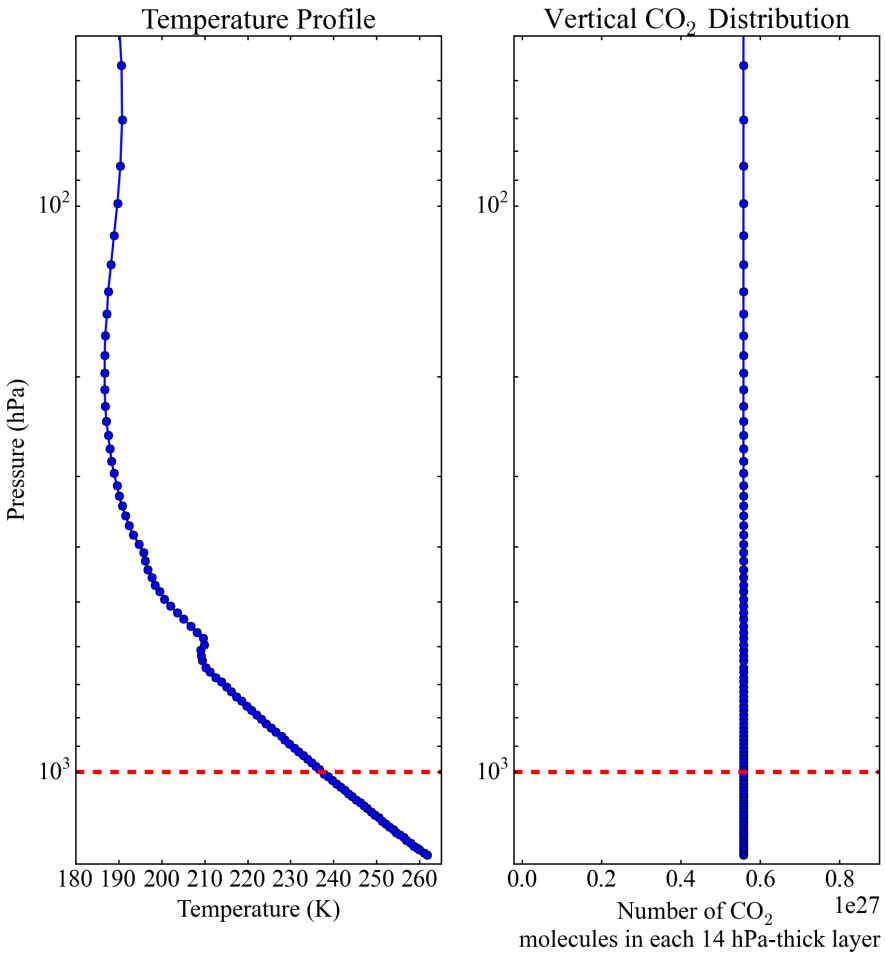

Figure 6.1: Reference temperature and CO_2 profiles with $p_{surf} = 1\,\text{bar} + p_{I,CO_2}$.
OLR $= 121.5\,\text{W m}^{-2}$; absorbed SW $= 121.5\,\text{W m}^{-2}$; $F_{net,TOA} = 0\,\text{W m}^{-2}$.

6.1 Three Different Approaches

With the reference equilibrium temperature profile with the correct surface pressure in place, the aim is to compare it to the case where the surface pressure is incorrectly fixed at 1 bar. Following are three ways that this result might be obtained.

6.1.1 Cloudsurface

One option is to leave everything fixed in place (i.e., the CO_2 molecules, the temperature profile, etc. all stay at the same pressure) and simply put an artificial surface in at the level where $p = 1\,\text{bar}$. The most important property of the surface is that it acts as a black body, which means that the temperatures of layers below it are unimportant to the radiative-convective equilibrium above it. To mimic this property, a cloud is placed in the layer at p = 1 bar. This cloud has a fraction of 1.0 and an optical depth of 999. This is illustrated in Figure 6.2. Since it is a cloud that mimics the properties of the surface, it is referred to as a 'cloudsurface'. The cloudsurface is non-transmissive to both SW and LW radiation.

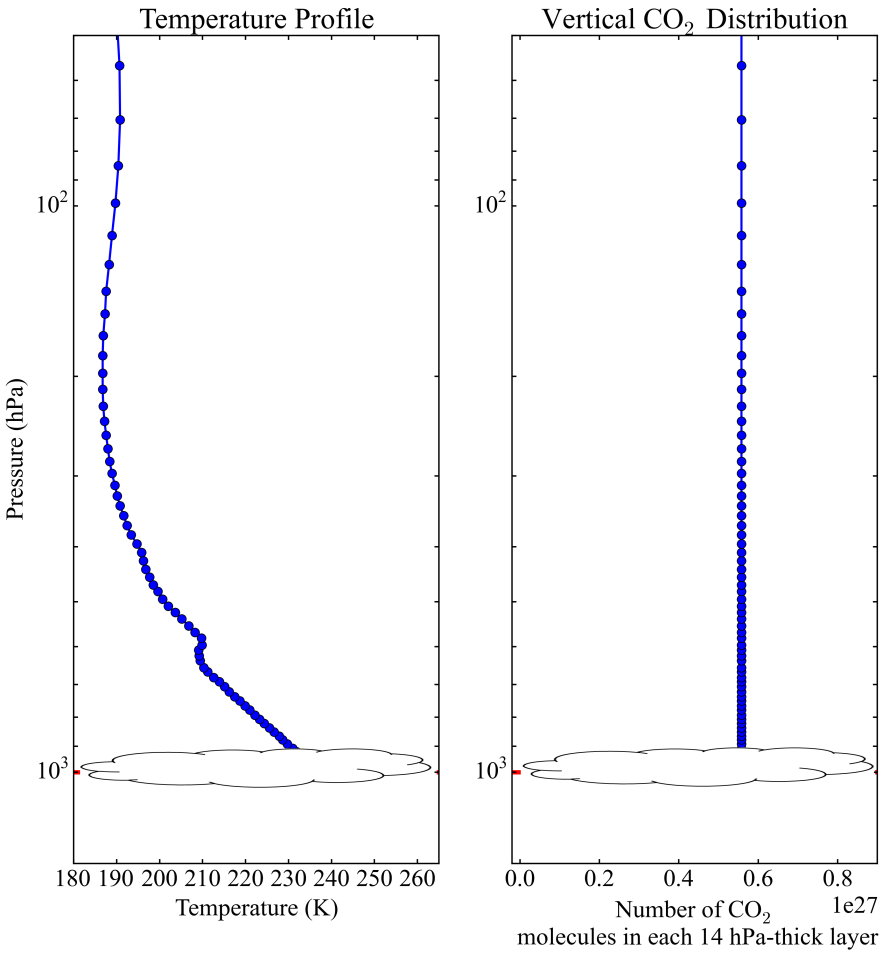

Figure 6.2: Temperature and CO_2 profiles with a cloudsurface at 1 bar. No atmospheric processes occur beneath the cloudsurface.
OLR = 109.7 W m^{-2}; absorbed SW = 109.7 W m^{-2}; $F_{net,TOA} = 0$ W m^{-2}

Since the layers beneath the cloudsurface no longer contribute to the OLR, it drops by 11.8 W m^{-2} to 109.7 W m^{-2}. However, the solar absorption also drops by 11.8 W m^{-2}. The reason for this is that the layers with $p >$ 1 bar are effectively no longer part of the atmosphere, since they are beneath the cloudsurface. Therefore, in the same way that any contributions to the OLR from this region are removed, so is any absorption of SW radiation by H_2O. This means that the atmosphere remains in radiative-convective equilibrium when the surface has moved from 1.4 bar to the cloudsurface at 1 bar, while the surface temperature has dropped from 263 K to the

cloudsurface temperature of 237 K. Because no atmospheric processes occur beneath the cloudsurface, it effectively *is* the surface. Therefore, the 'surface temperature' in an atmosphere containing a cloudsurface is the cloudsurface temperature[1].

Now this process can be pictured in reverse. The atmosphere is in radiative-convective equilibrium with the surface (the cloudsurface) at 1 bar. The cloudsurface is then moved downward from $p = 1$ bar to $p = 1.4$ bar. The convective adjustment is applied as in Chapter 3, so the adiabat is followed all the way down to $p = 1.4$ bar. The surface temperature increases by 26 K, but OLR still equals the absorbed SW, so the atmosphere remains in equilibrium. This 26 K warming is caused by the extension of the troposphere into the layers with $p > 1$ bar — this is convective deepening.

With 0.4 bar of CO_2, adding a cloudsurface did not change the TOA net flux. For smaller CO_2 inventories, the TOA net flux changed slightly with the addition of a cloudsurface, but not significantly (by no more than $2\,\mathrm{W\,m^{-2}}$).

The cloudsurface behaves identically to the actual surface, so the two situations depicted in Figure 6.3 are equivalent. The cloudsurface is employed in this study for ease of use.

[1]The albedo of the cloudsurface is set to the surface albedo of the atmosphere into which it is placed, so it also acts like the surface with respect to shortwave radiation.

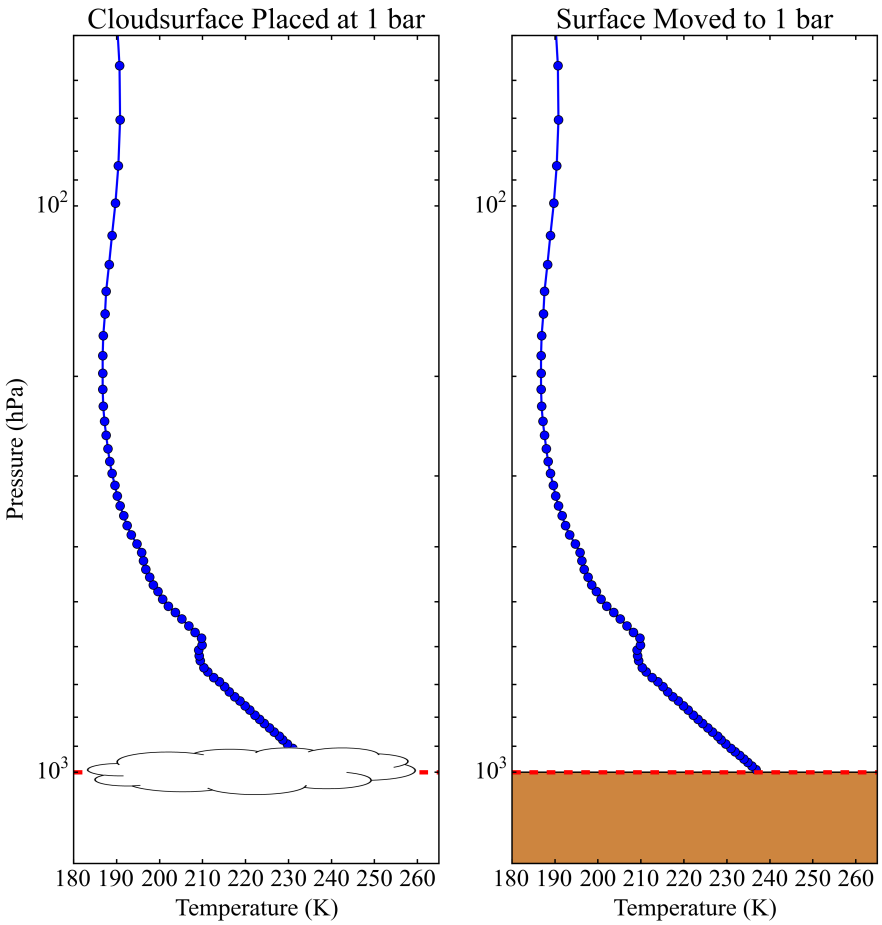

Figure 6.3: Illustration of the equivalence of placing a cloudsurface at 1 bar and moving the surface to 1 bar. The top of the brown area represents the surface.

6.1.2 Addition of Radiatively Inert Gas

Another option is to take the reference equilibrium temperature profile from Figure 6.1, remove all of the radiatively active gas molecules (CO_2, H_2O, and O_3) from the layers with $p > 1$ bar, and replace them with an equivalent mass of a radiatively inert gas such as N_2. This is illustrated in Figure 6.4.

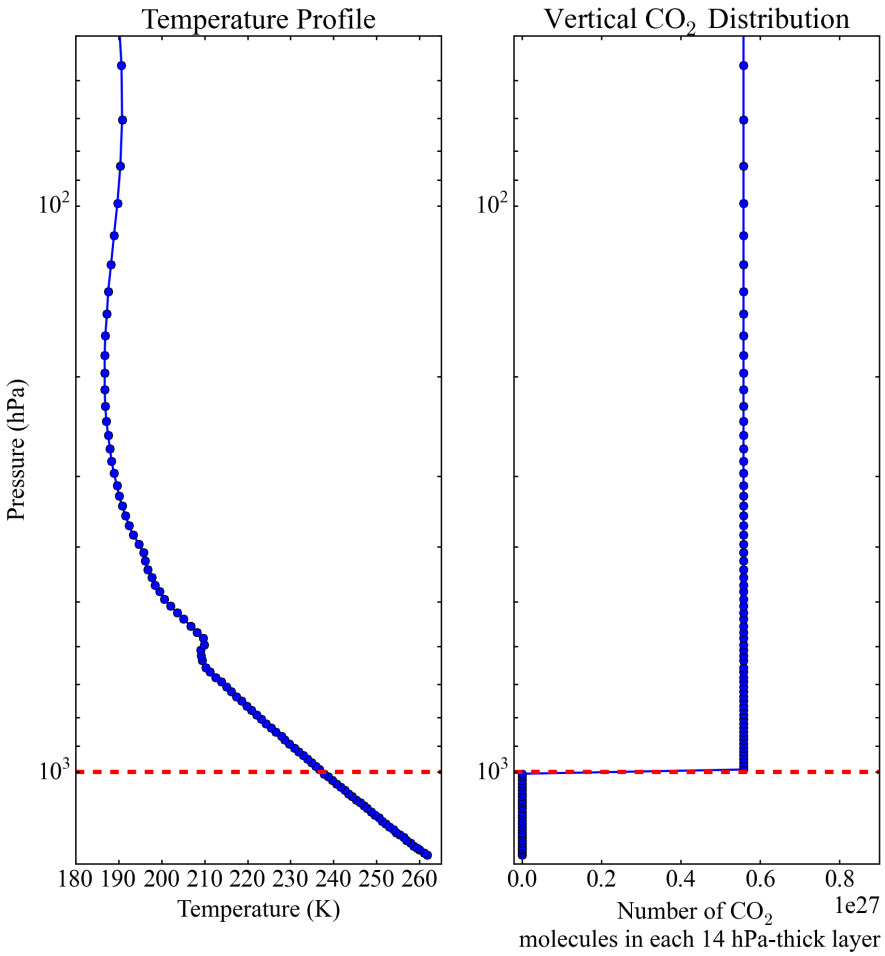

Figure 6.4: Temperature and CO_2 profiles with the radiatively active gas removed from layers with $p > 1$ bar and replaced with radiatively inert N_2. OLR = 126.4 W m^{-2}; absorbed SW = 109.7 W m^{-2}; $F_{net,TOA} = 16.7$ W m^{-2}

The purpose of the inert gas is to increase the surface pressure without increasing the number of CO_2 molecules, so that the effect of the increased pressure can be isolated.

However, the OLR thus obtained is 126.4 W m^{-2}, which is an *increase* of 4.9 W m^{-2} compared to Figure 6.1. Meanwhile, the solar absorption has decreased by 11.8 W m^{-2} as it did with the cloudsurface, since all the water vapour molecules for $p > 1$ bar have been removed. There is now a discrepancy of 16.7 W m^{-2} between absorbed SW and OLR.

When comparing the temperature profiles in Figure 6.4 and Figure 6.2,

there are two differences, either of which could cause this discrepancy. One is the higher surface temperature, which is still 263 K with the inert gas added vs. 237 K with the cloudsurface. The other difference is the emission of the atmospheric layers (not the surface) where $p > 1$ bar, which cannot contribute to the OLR when the cloudsurface is in place, but might be doing so here.

This can be investigated by changing each in turn. First, the temperature of every atmospheric layer with p > 1 bar (but not the surface) is set to 237 K, which creates an isotherm downwards from $p = 1$ bar. This is shown in Figure 6.5.

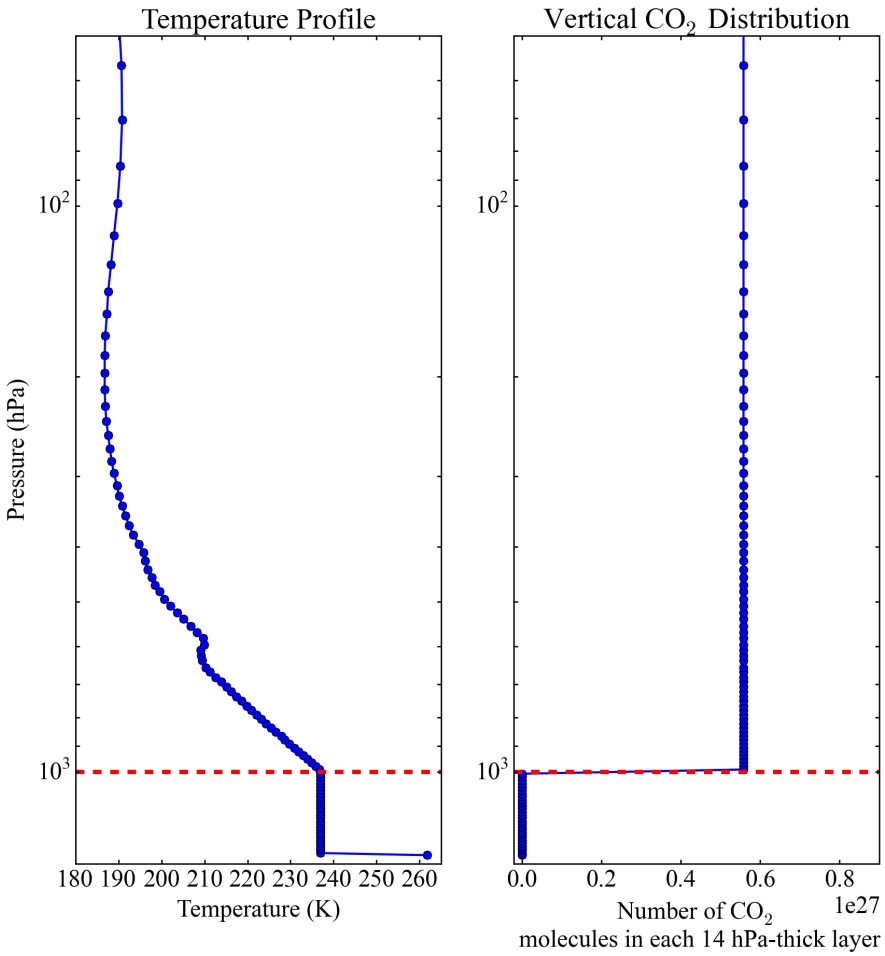

Figure 6.5: Temperature and CO_2 profiles with the layers where $p > 1\,\text{bar}$ (but not the surface) set to an isotherm downward from $p = 1\,\text{bar}$ so that they do not contribute to the OLR.
OLR $= 126.4\,\text{W m}^{-2}$; absorbed SW $= 109.7\,\text{W m}^{-2}$; $F_{net,TOA} = 16.7\,\text{W m}^{-2}$

The OLR is unchanged at $126.4\,\text{W m}^{-2}$, so these layers are not the source of the discrepancy between the OLR and the absorbed SW.

Second, the temperatures of these layers revert to following the adiabat as before, but the surface temperature is decreased to the temperature at $p = 1\,\text{bar}$, which is 237 K. This is shown in Figure 6.6.

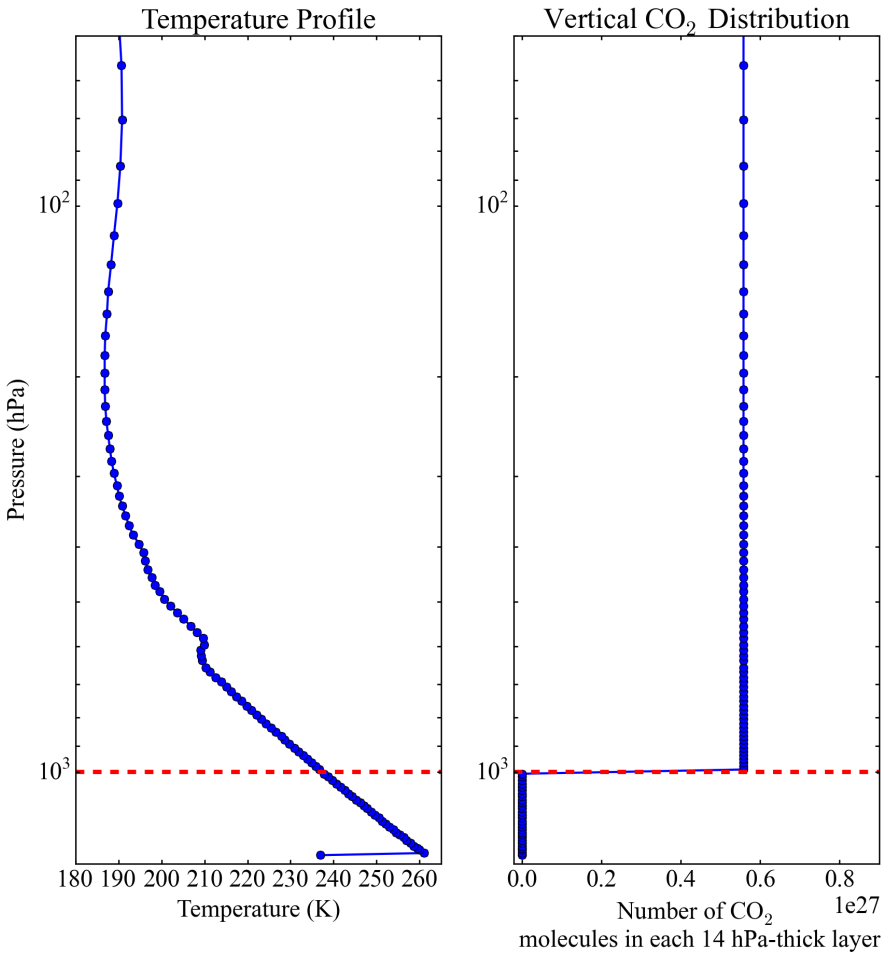

Figure 6.6: Temperature and CO_2 profiles as in Figure 6.4 but with the surface temperature set to the temperature at $p = 1$ bar, which is 237 K. OLR = 109.7 W m^{-2}; absorbed SW = 109.7 W m^{-2}; $F_{net,TOA} = 0$ W m^{-2}

The OLR is 109.7 W m^{-2}, which now matches the absorbed SW radiation. The atmosphere is now in equilibrium. This matches exactly the result from Figure 6.2 with the cloudsurface at 1 bar.

So the reason for the discrepancy between the OLR and the absorbed SW when all the radiatively active gas in the region where $p > 1$ bar is replaced with N_2 as in Figure 6.4 was that the surface temperature was artificially high. There is a disconnect between the CO_2 profile, which stops at 1 bar, and the temperature profile, which continues down until $p = 1 + p_{I,CO_2}$, to 263 K. So the cloudsurface is the better method for modelling the surface

temperature when the surface pressure is 1 bar, since it avoids this incorrectly high surface temperature.

6.1.3 Constant Number of CO_2 Molecules

One might think that the way to compare the effect of either fixing or increasing the surface pressure for an atmosphere with 0.4 bar of CO_2 molecules would be to keep the *number* of CO_2 molecules fixed. However, the important thing is not the total number of CO_2 molecules, but their distribution.

For example, we can calculate the number of CO_2 molecules in the reference atmosphere in Figure 6.1

$$N_{CO_2} = \frac{Ap_{I,CO_2}N_A}{gM_{CO_2}} = \frac{1 \times 0.4 \times 10^5 \times 6.022 \times 10^{23}}{9.81 \times 44.01 \times 10^{-3}} = 5.58 \times 10^{28} \text{ molecules}$$

where A is the area of the column in question, which in this model is $1\,\mathrm{m}^2$.

These molecules are spread equally across the 100 layers (which have equal pressure thickness of 14 hPa). In the extreme case where all of these CO_2 molecules were moved down to the layer directly above the surface, where the temperature is $\approx 262\,\mathrm{K}$, the OLR would clearly be significantly higher than its value of $121.5\,\mathrm{W\,m^{-2}}$ when the molecules are evenly distributed, so the distribution of the CO_2 molecules, and not just the total number, is important.

Figure 6.7 shows what happens when one takes the reference atmosphere from Figure 6.1, moves the surface to 1 bar, and keeps the number of CO_2 molecules constant: the number of molecules in the region where $p < 1\,\mathrm{bar}$ increases, so the number of molecules per 14 hPa-thick layer increases. Since our aim is to show what happens when the surface pressure changes *while everything else remains unchanged*, the approach of keeping the number of CO_2 molecules constant is not appropriate.

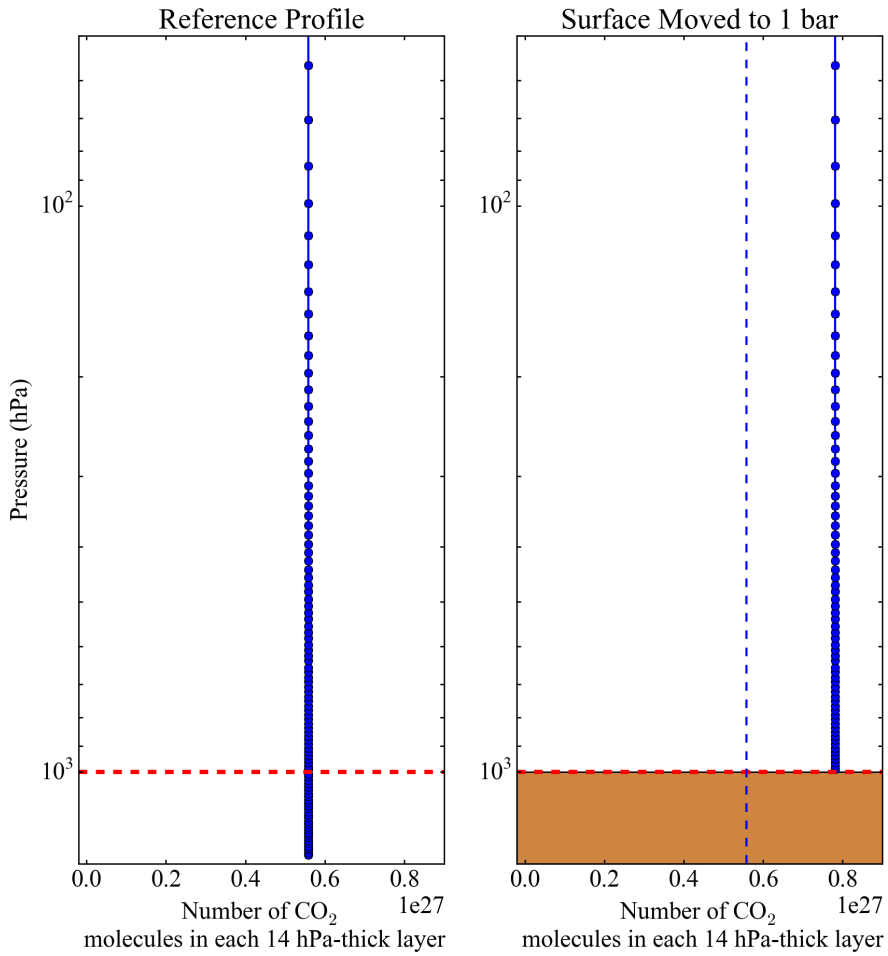

Figure 6.7: The left-hand figure shows the CO_2 distribution as in Figure 6.1. OLR = 121.5 W m^{-2}; absorbed SW = 121.5 W m^{-2}; $F_{net,TOA} = 0$ W m^{-2}; In the right-hand figure, the surface has been moved to $p = 1$ bar. The blue dashed line shows the CO_2 distribution as in Figure 6.1. The solid blue line shows the CO_2 distribution when all of the CO_2 molecules from the region where $p > 1$ bar are moved to the region where $p < 1$ bar.
OLR = 105.0 W m^{-2}; absorbed SW = 109.7 W m^{-2}; $F_{net,TOA} = -4.7$ W m^{-2}

6.1.4 Conclusions

The only method that actually allows a comparison between a realistic atmosphere with a surface pressure of 1 bar and one with surface pressure of 1.4 bar is the cloudsurface method. Adding a radiatively inert gas results

in an artificially high surface temperature, while using a constant number of CO_2 molecules changes the CO_2 distribution in the region where $p < 1\,\text{bar}$ in an unintended way.

6.2 Relative Importance of Pressure Broadening and Convective Deepening

It has been shown above that increasing the surface pressure increases the surface temperature because convection extends into deeper layers. However, increasing the surface pressure also increases the pressure broadening. This would cause the surface temperature to increase even without convective deepening. This effect was investigated by Hu et al. [15], but they attributed *all* of the warming to pressure broadening.

In my model, it is possible to test the warming effect of pressure broadening separately from convective deepening. For an atmosphere in equilibrium with $p_{surf} = 1 + p_{I,CO_2}$, the value of p that is used in selecting the correlated-k distribution for a given layer can be reduced through multiplication by a factor of $\frac{1}{1+p_{I,CO_2}}$. This means that, for the radiative routine, the surface pressure is now 1 bar, while the pressure for the other layers is also scaled appropriately. For the atmospheric structure routine, the pressures are left unchanged. Figure 6.8 shows two correlated-k distributions at different pressures, and demonstrates that the absorption will be greater for the case with higher pressure.

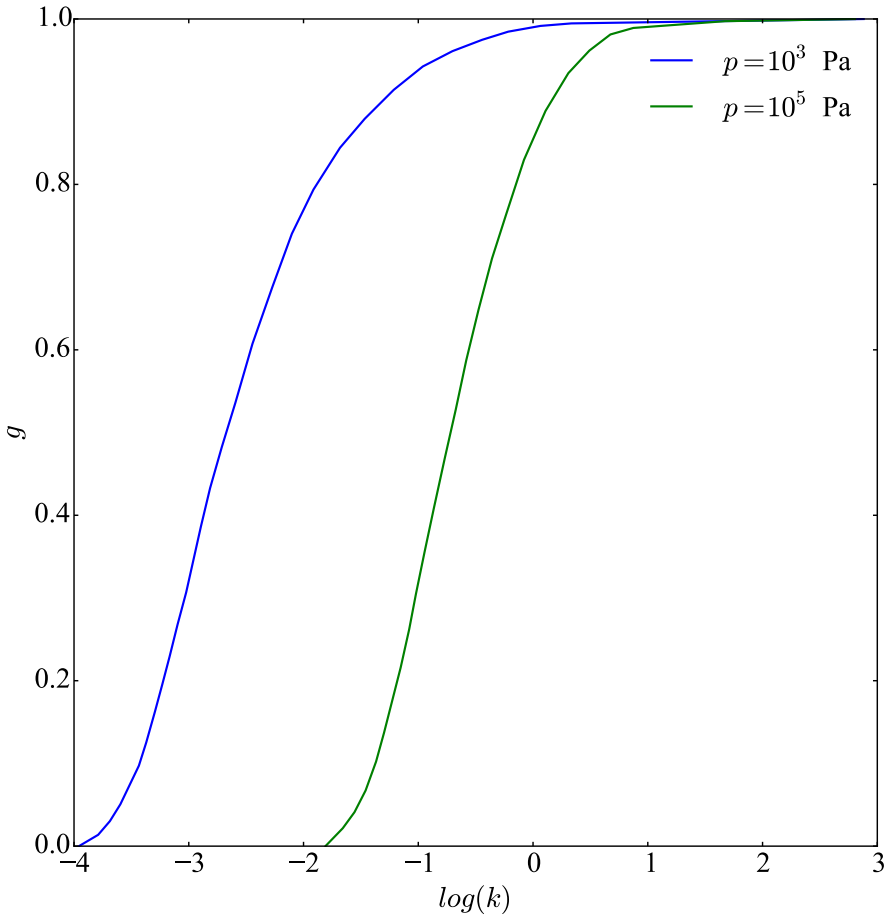

Figure 6.8: The effect of pressure broadening on a correlated-k distribution. The increased pressure means an increased probability of a high absorption coefficient. (Figure from Lacis and Oinas [21]).

With pressure broadening turned off, the OLR increases. The surface temperature must then decrease to compensate. The new equilibrium surface temperature is obtained, and the difference between the two represents the warming that can be attributed exclusively to pressure broadening. The surface temperatures in each case are shown in Figure 6.9. The surface warming relative to the case with neither pressure broadening nor convective deepening is shown in Figure 6.10.

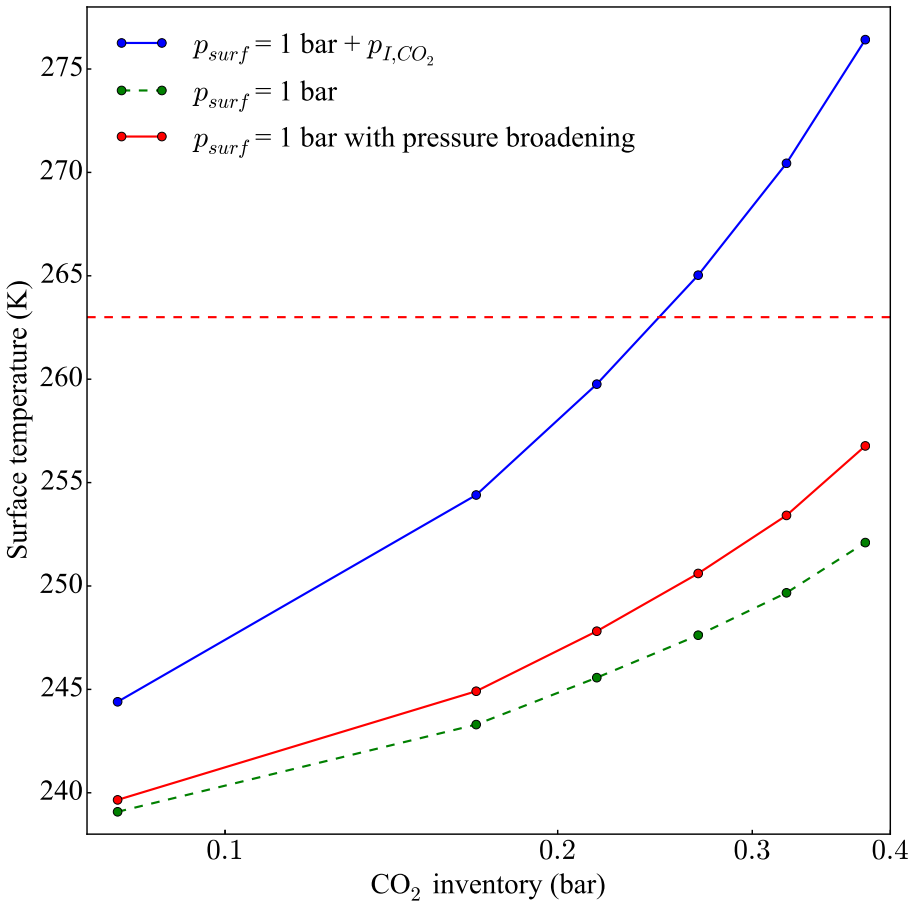

Figure 6.9: The surface temperature with both pressure broadening and convective deepening (blue), with pressure broadening only (red), and with neither (green). The dashed red line is at 263 K, where deglaciation occurs.

Another approach to calculating the warming effect of pressure broadening is to take an atmosphere with $p_{surf} = 1$ bar and *increase* the pressure for the radiative routine. This decreases the OLR, resulting in an increased equilibrium surface temperature. This approach was tested and gave the same result as the earlier method, so this earlier method, which is slightly more intuitive, is used.

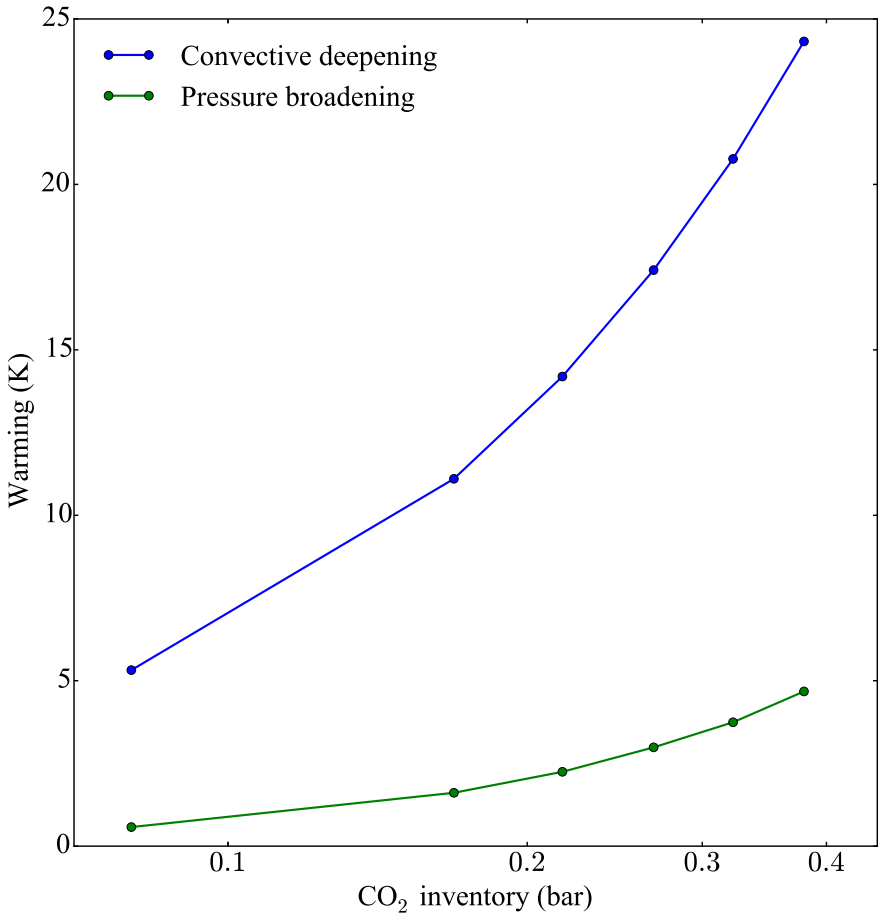

Figure 6.10: Comparison of the warming effects of both pressure broadening and convective deepening

As noted by Hu et al. [15], pressure broadening becomes an increasingly important warming mechanism as the CO_2 inventory increases. This is evident in Figure 6.11, which shows the pressure broadening warming as a fraction of the total warming. However, for CO_2 inventories smaller than 0.35 bar (and presumably somewhat greater than that, given the trend for inventories up to 0.35 bar), convective deepening is the dominant warming mechanism when the surface pressure is increased.

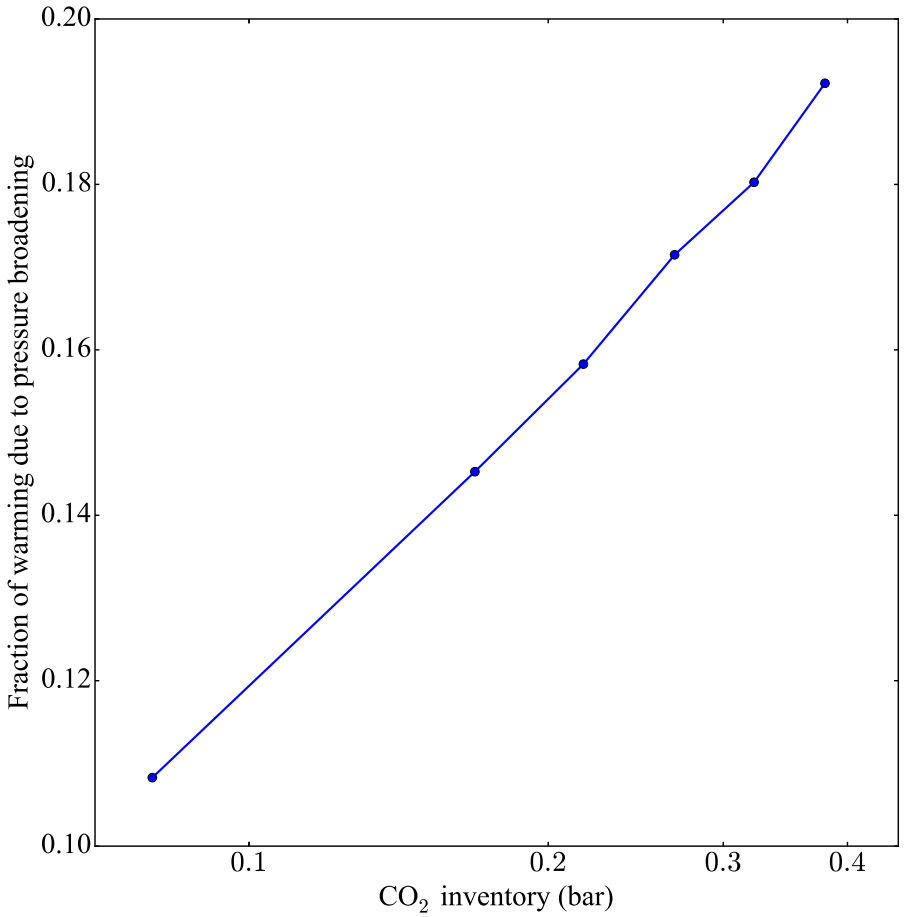

Figure 6.11: Pressure broadening warming as a fraction of total warming

CHAPTER 7

Atmospheric Composition Effects

Clearly, the change in surface pressure is the most important consequence of the change in atmospheric composition caused by the addition of a large CO_2 inventory. However, there are other consequences, which are explored below.

7.0.1 Specific Heat at Constant Pressure

The specific heat at constant pressure, c_p, is an important quantity to calculate accurately. This is due to its effect on the moist adiabatic lapse rate. The specific heat of air at constant pressure is $1.004\,\mathrm{kJ\,kg^{-1}\,K}$, and stays fairly constant within the normal range of atmospheric temperatures. For CO_2, in contrast, c_p depends on temperature through the relation $c_{p,CO_2} = 0.0011T + 0.5177$, with T in Kelvin. With $p_{I,CO_2} = 0.25\,\mathrm{bar}$, $c_{p,tot}$ for a temperature of 263 K drops from $1.004\,\mathrm{kJ\,kg^{-1}\,K}$ to $0.98\,\mathrm{kJ\,kg^{-1}\,K}$.

7.0.2 Specific Gas Constant

The specific gas constant $R_{specific}$ is $286.9\,\mathrm{J\,kg^{-1}\,K}$ for dry air, and $188.9\,\mathrm{J\,kg^{-1}\,K}$ for CO_2. In an atmosphere with a CO_2 inventory of 0.25 bar, $R_{specific}$ drops by 5% to $270.0\,\mathrm{J\,kg^{-1}\,K}$.

The changes to $R_{specific}$ and c_p mean that the moist adiabatic lapse rate increases from $9.8\,\mathrm{K\,km^{-1}}$ to $10.3\,\mathrm{K\,km^{-1}}$. This results in the surface temperature increasing by 2.2 K; the temperature profile is shown in Figure 7.1.

The tropopause remains at a fixed height, and the temperature increase is caused by the steeper lapse rate.

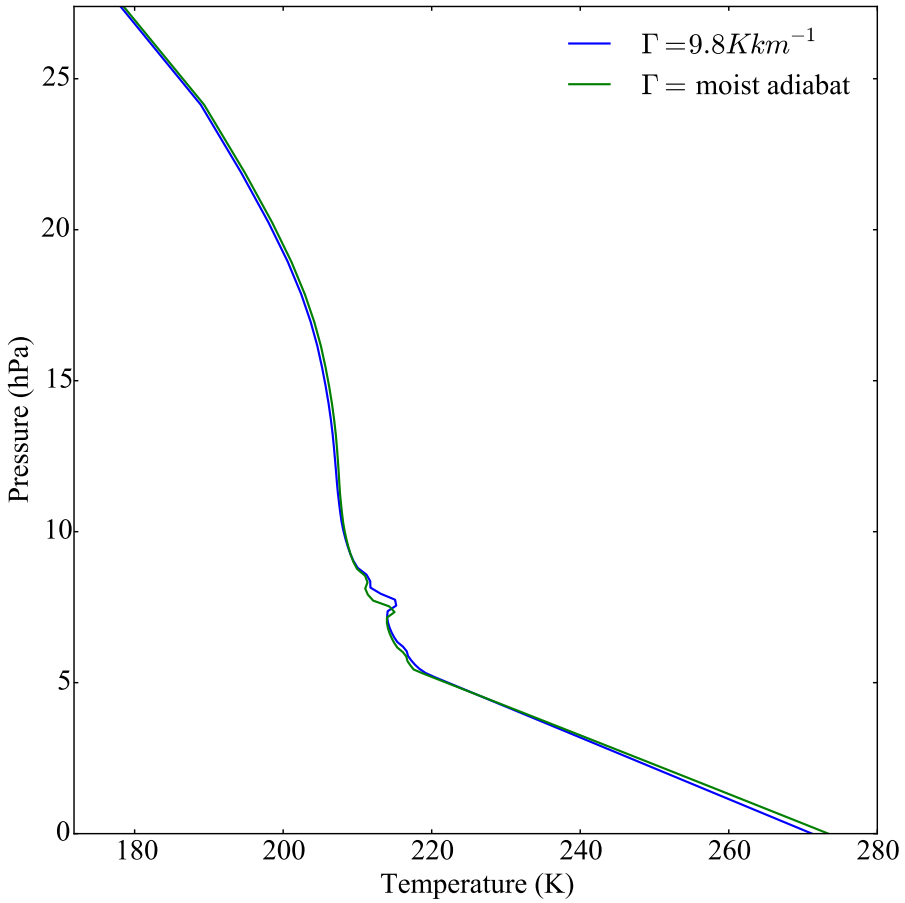

Figure 7.1: The effect of changing c_p and $R_{specific}$ on the temperature profile

7.0.3 Mean Molecular Weight

The mean molecular weight of the Earth's atmosphere is typically stated to be around $29.0\,\mathrm{g\,mol^{-1}}$. However, mean molecular weight is a function of CO_2 inventory, as shown in Figure 7.2. With a CO_2 inventory of 0.4 bar, the mean molecular weight is $32.1\,\mathrm{g\,mol^{-1}}$, an increase of 11%. This would cause the number of total molecules in the atmosphere to be overestimated by 11%. This could cause an error, depending on the model. For example,

in my model this would cause the number of 'broadening molecules' to be overestimated. This is an input to PRRTM, which is used to calculate the foreign broadening of CO_2 absorption lines by N_2 and O_2, so overestimating the total number of molecules would cause the foreign broadening to be overestimated.

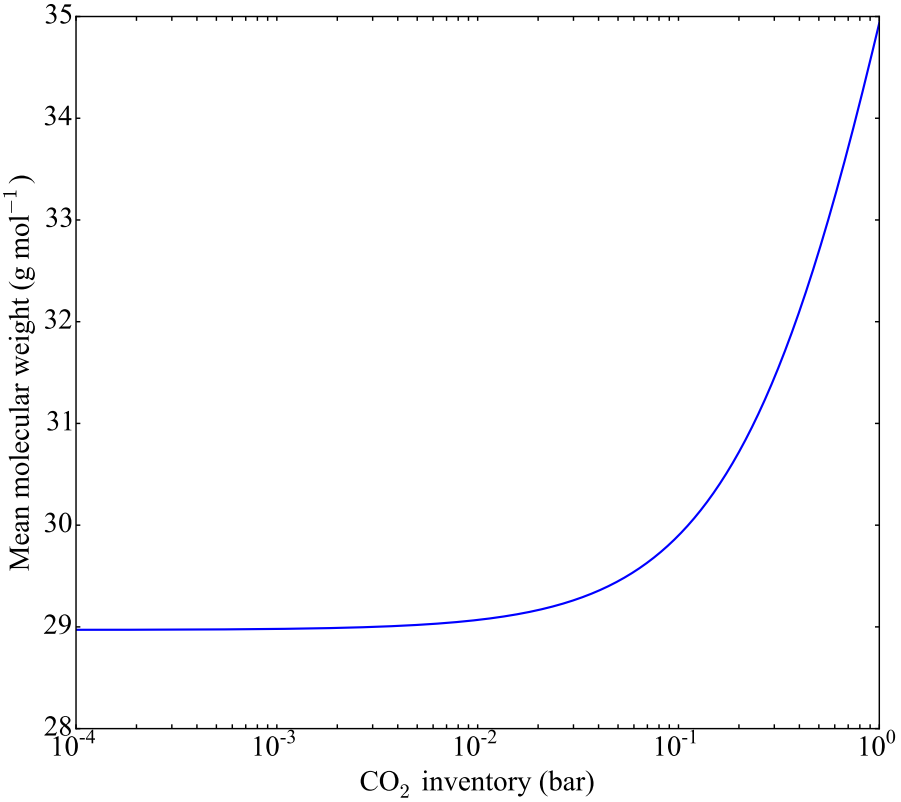

Figure 7.2: The effect of the CO_2 inventory on the mean molecular weight of the atmosphere

CHAPTER 8

Equilibrium States and Evolution of the System

For a given inventory of CO_2, Earth's atmosphere can have multiple equilibrium surface temperatures. This is due to the fact that the planet is covered with water, which can have very different albedos when liquid and frozen. Two extreme states are possible — a planet with no ice (the 'hothouse' state) and a planet covered entirely with ice (the Snowball state). In the transition from Snowball to hothouse, it is also possible (depending on various parameters) to reach an unstable equilibrium state in which the planet is partially covered with ice. This is the state of the Earth in the present day.

In the preceding chapters we examined the effect of increased surface pressure on the transition out of the Snowball state; in this chapter we explore its effect on the whole range of possible states.

8.1 Ice-Albedo Feedback

One way to define the degree of glaciation is the ice-line, which is the latitude to which the ice reaches. In a Snowball state, the ice-line is close to 0°, and in a hothouse state the ice-line is at 90°. In order to describe the transition between the two extreme states, we need to know how the ice-line retreats in response to an increase in global average temperature. For our purposes, the position of the ice-line is important because it determines the albedo of the planet. Pierrehumbert et al. [19] provide the following form for albedo

as a function of global average surface temperature

$$\alpha(T) = \begin{cases} \alpha_i & \text{for } T \leq T_i, \\ \alpha_0 + (\alpha_i - \alpha_0)\frac{(T-T_0)^2}{(T_i-T_0)^2} & \text{for } T_i < T < T_0, \\ \alpha_0 & \text{for } T > T_0 \end{cases} \tag{8.1}$$

where α_0 is the planetary albedo when there is no ice and α_i is the ice albedo. T_i and T_0 are critical temperatures such that if $T < T_i$ the planet is completely ice-covered, while if $T > T_0$ the planet is completely ice-free.

As shown in Figure 8.1, the rate of change of albedo with temperature is large when moving away from an ice-covered planet and smaller when moving toward an ice-free planet. This is because the ice starts to melt at the equator, where the insolation is highest, while the final ice to melt is at the poles, where the insolation is lowest.

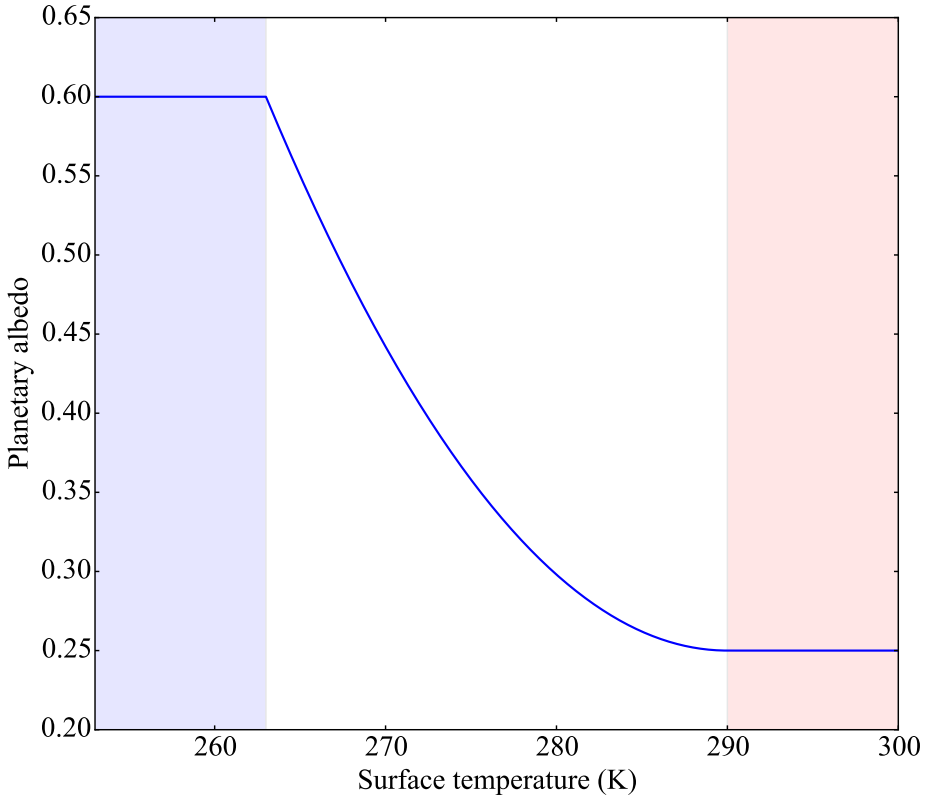

Figure 8.1: Planetary albedo as a function of temperature from Pierrehumbert et al. The region shaded blue represents a fully ice-covered planet and the region shaded red represents an ice-free planet.

From this, the absorbed SW radiation as a function of temperature can be calculated

$$F_{SW}(T) = \frac{F_0}{4}(1 - \alpha(T)) \tag{8.2}$$

Equation 8.2 encapsulates all the information about SW absorption. Previously, we defined the atmosphere to be in equilibrium when the OLR was equal to the total SW absorption as calculated using Lacis and Hansen's [22] parameterisation; in this chapter, equilibrium is reached when the OLR is equal to the absorbed SW as given by Equation 8.2 (or rather, the modified version Equation 8.3). This simplification allows us to move beyond the validated range of Lacis and Hansen's parameterisation and explore a wider phase space. The heating rates are still calculated using Lacis and Hansen's parameterisation.

The constant planetary albedo in the Snowball state in Equation 8.1 means a constant amount of absorbed SW radiation for temperatures less than 263 K. However, this is not completely realistic; as the surface temperature increases, the amount of water vapour increases, and so the amount of SW radiation absorbed by water vapour increases. Some of this radiation would have been absorbed by the surface, so the surface absorption decreases, but the total SW absorption increases with surface temperature. Figure 8.2 shows the SW absorption in the range 230–263 K in the radiative-convective model using Lacis and Hansen's parameterisation.

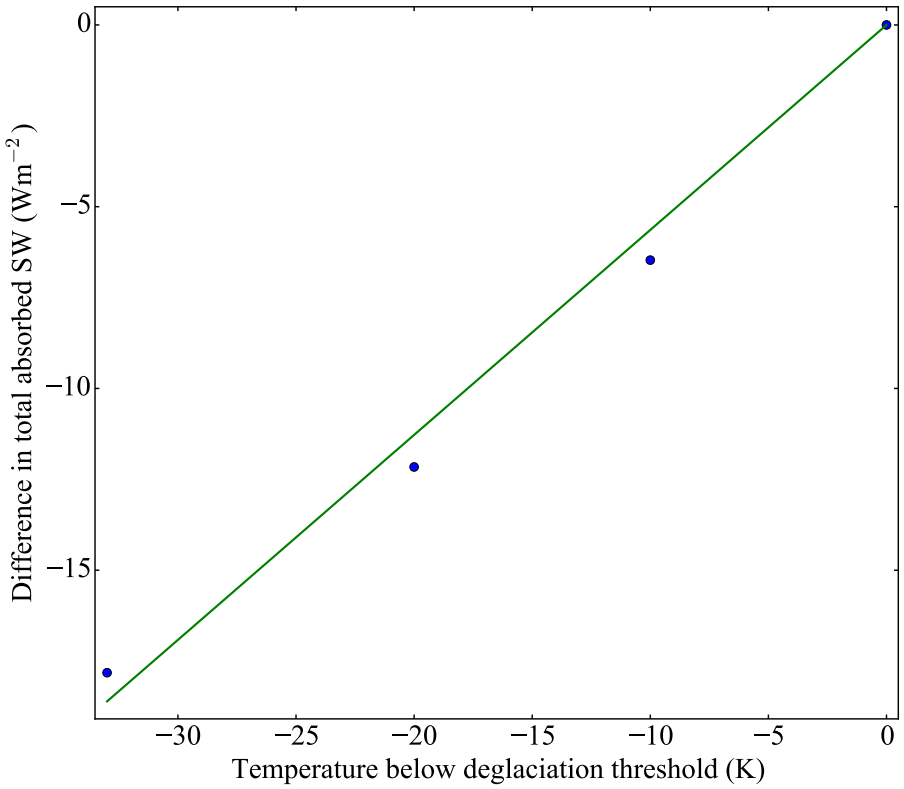

Figure 8.2: SW absorption as a function of temperature calculated using the radiative-convective model with Lacis and Hansen's SW parameterisation. Both the SW absorption and temperature are plotted relative to their values at deglaciation.

The absorbed SW is clearly not constant with temperature. From this figure, a linear relationship can be obtained between surface temperature and

total solar absorption. The line of best fit has a slope of 0.194, so a correction is made to Equation 8.2:

$$F_{SW}(T) = \frac{F_0}{4}(1 - \alpha(T)) + 0.194(T - 263) \tag{8.3}$$

This correction is made only to the Snowball branch (i.e. when $T < 263\,\mathrm{K}$), in order to ensure that the deglaciation curve in the bifurcation diagram behaves similarly to the way it does in the full model where the absorbed SW radiation is calculated more realistically. In the hothouse branch, which is somewhat outside the valid range of Lacis and Hansen's parameterisation, we leave the albedo as it is in the formulation from Pierrehumbert et al.

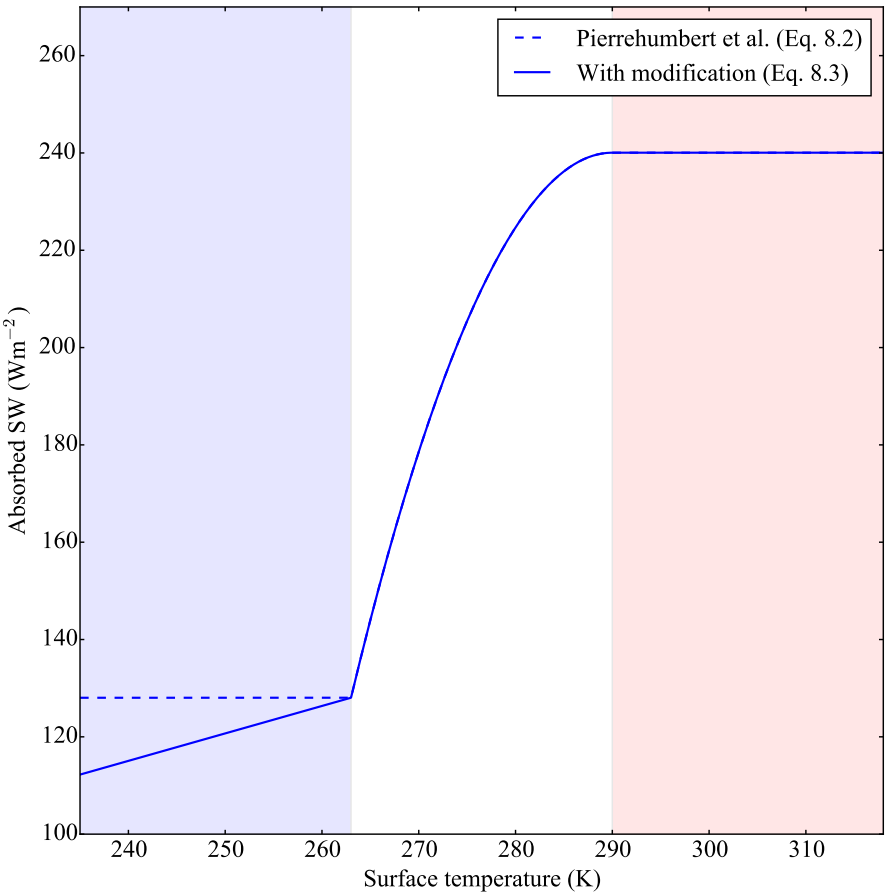

Figure 8.3: SW absorption as a function of temperature from Equations 8.2 and 8.3. The region shaded blue represents a fully ice-covered planet, and the region shaded red represents an ice-free planet.

8.2 Equilibrium States

8.2.1 Types of Equilibrium

Three types of equilibrium are possible for Earth's ocean-atmosphere system. The first is the Snowball state that is the focus of this thesis. During this state, the planet is entirely or near-entirely covered in ice (the distinction here is very important to the survival of life through a Snowball state, which

is an area of active debate [4][2], but is not crucial to our examination of deglaciation).

The second is the hothouse state. This occurs in the aftermath of a Snowball. At the point of deglaciation, there is a large amount of CO_2 in the atmosphere. The ice melts much more quickly than the CO_2 is drawn down out of the atmosphere, which results in a planet with low albedo (and therefore a large amount of SW absorption) and a large greenhouse effect. This causes the surface temperature to increase greatly – aided by water-vapour feedback, it can reach in excess of 300 K. The hothouse state is therefore very warm and wet, with a large atmospheric inventory of CO_2. This makes it somewhat difficult to model, since many of the familiar parameters are pushed to their extremes. For this reason, the specific temperatures in the hothouse state as modelled here should be regarded as the least certain; nonetheless, the overall phase space and the influence of convective deepening on this phase space should be acceptably accurate.

The final type of equilibrium is an unstable, partially ice-covered state somewhere between a hothouse and a Snowball. The reason for its instability can be seen in Figure 8.4. The net flux is the absorbed SW minus the OLR, so a negative value means that the planet emits more flux than it receives. For the unstable state b, a perturbation to the left (to a lower temperature) results in a negative net flux, which means the planet must cool further to restore the net flux to zero. This results in a feedback that takes the system all the way to state a, which is a Snowball state. A perturbation from state b in the other direction would similarly take the system into state c, a hothouse state.

In contrast, a perturbation to the right from state a results in a negative net flux, which requires the system to cool to regain equilibrium, which leads it back into state a. The same argument holds for state c, which is why these states are stable states.

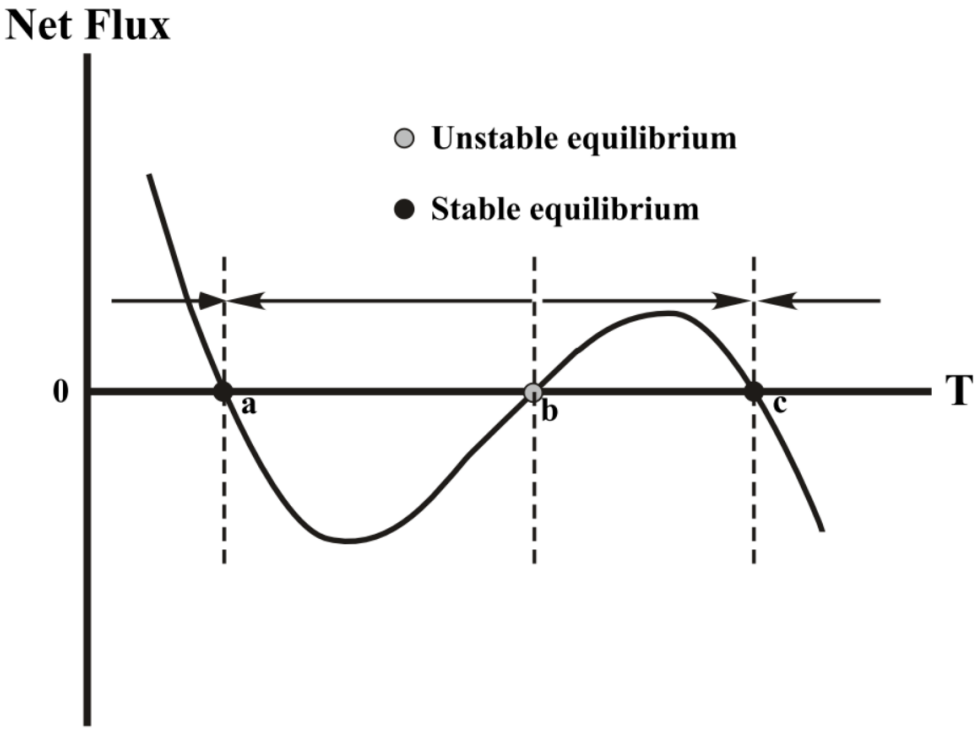

Figure 8.4: Stability of equilibrium solutions. Figure from Pierrehumbert [39].

8.2.2 Finding Equilibria

To explore these states, we use the model to obtain curves of surface temperature versus OLR for various CO_2 inventories. To simplify the task, these calculations are performed with a clear sky, and a constant reduction to the OLR of $15.66\,\mathrm{W\,m^{-2}}$ is made to account for LW cloud forcing, as in Hu et al [15]. This simplification is necessary because of the wide range of temperatures and CO_2 inventories that are examined throughout the process, for which there is no simple parameterisation of cloud forcing.

On the same axes, we plot the absorbed SW radiation from Equation 8.3. Anywhere that the OLR is equal to the absorbed SW is an equilibrium state of the atmosphere. For a given CO_2 inventory, up to three equilibria are possible. This is illustrated in Figure 8.5.

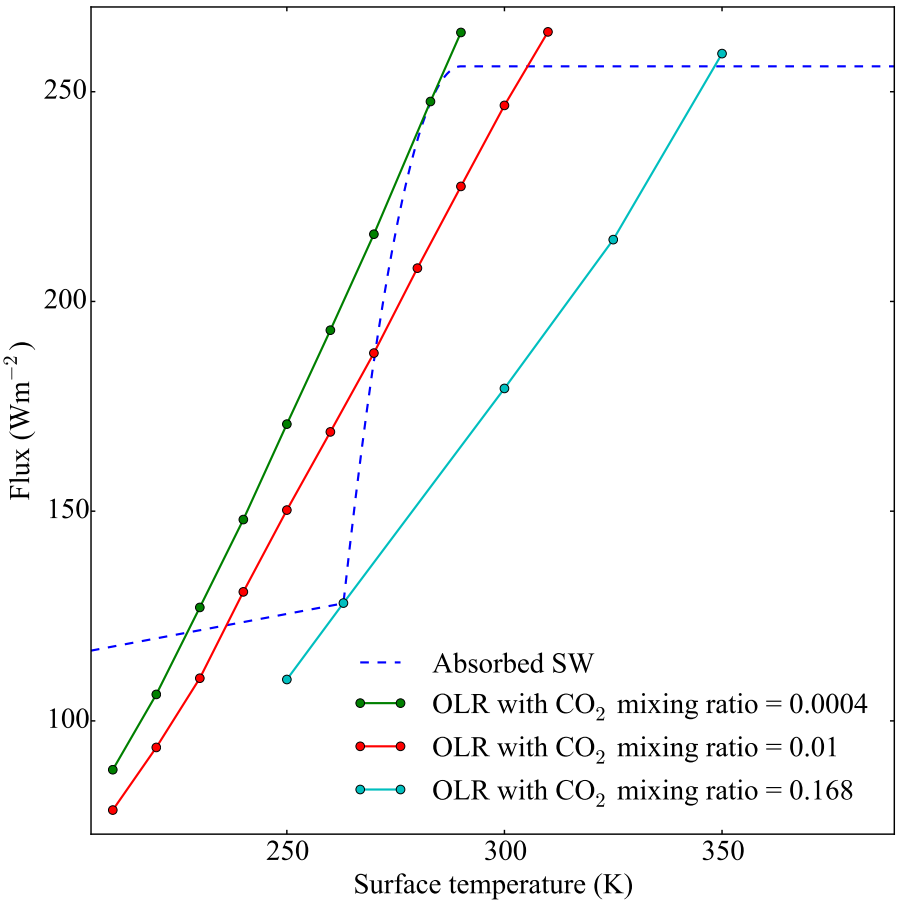

Figure 8.5: OLR curves for various CO_2 mixing ratios

With a mixing ratio of 0.01, the OLR is equal to the absorbed SW at a temperature of 236 K. Since the temperature is less than 263 K, this is a Snowball state. The OLR is also equal to the absorbed SW at 272 K, which is an unstable equilibrium. Finally, the OLR curve also crosses the absorbed SW curve at 297 K, which represents a hothouse state. Therefore, with a mixing ratio of 0.01, all three equilibrium states are possible.

These three equilibria are not possible for every CO_2 mixing ratio, however. For instance, when the mixing ratio is 0.0004 there is a Snowball equilibrium state at 233 K, but there is no other equilibrium. There is very nearly an equilibrium at 283 K, but the OLR is slightly greater than the absorbed SW.

At a slightly higher CO_2 mixing ratio, there would be a equilibrium at 283 K. If the mixing ratio was then reduced to 0.0004, there would no longer be an equilibrium state at a nearby temperature, and the system would have to drop down to 233 K to find a new equilibrium. In this way, a very small reduction in the CO_2 inventory could cause a drop in temperature of 56 K. This represents the onset of a glaciation.

At the other end of the scale, with a mixing ratio of 0.168, there is a Snowball equilibrium at 262.9 K. If the mixing ratio is increased slightly, there is no equilibrium state possible until the temperature is 350 K.

The post-deglaciation temperature of 350 K may be something of an overestimate; a fixed surface relative humidity of 80% is used throughout, which may not hold at these very high temperatures. Other similar approximations may also break down. Qualitatively, however, the aim is to show that the discontinuous response of temperature to a small change in CO_2 mixing ratio is again evident. The full range of equilibrium states of the atmosphere is best explored with a bifurcation diagram.

8.3 Bifurcation

A bifurcation diagram shows the discontinuous change in a variable (in our case, surface temperature) when a 'bifurcation parameter' (CO_2 inventory) is smoothly varied. To construct a bifurcation diagram, the OLR as a function of surface temperature is plotted for several different values of CO_2 inventory, and the equilibrium solutions are obtained as in Figure 8.5. These are then plotted against the CO_2 inventory, as shown in Figure 8.6.

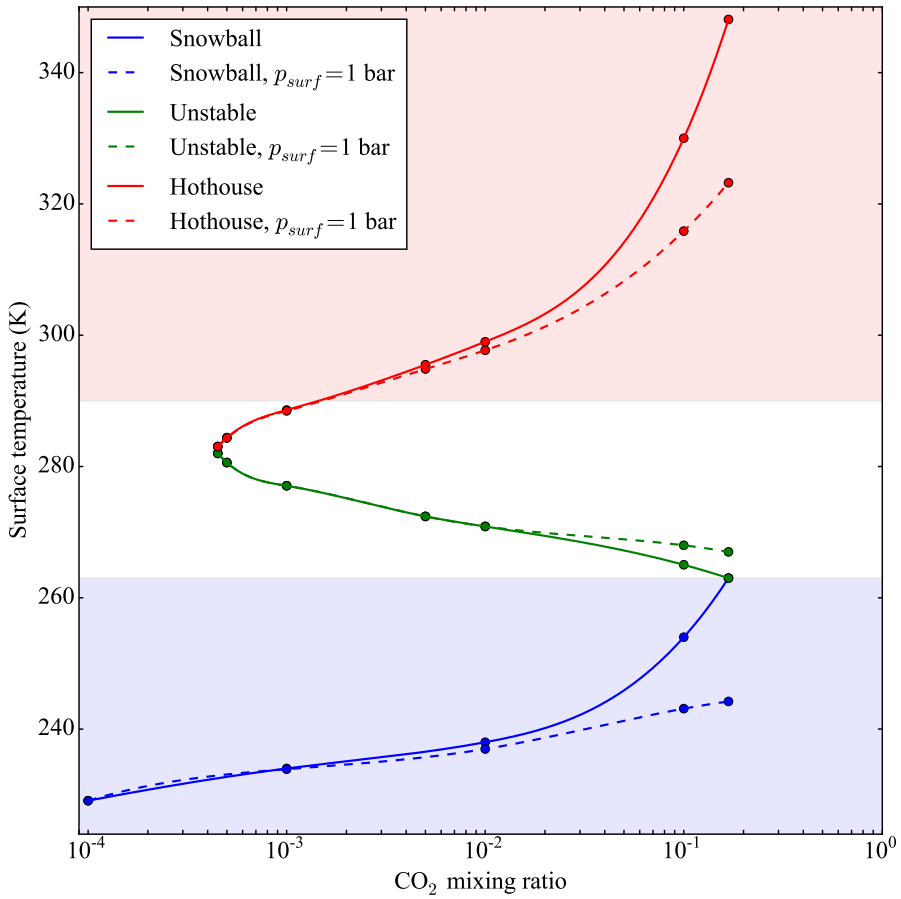

Figure 8.6: Bifurcation diagram. The equilibrium solutions (both stable and unstable) are shown within the overall phase space. The region shaded blue represents a fully ice-covered planet, and the region shaded red represents an ice-free planet. The dashed lines are the solutions without convective deepening.

The process is repeated with the surface held at 1 bar. The resulting equilibrium temperatures are shown with the dashed lines in Figure 8.6.

The deglaciation threshold can be read easily from the figure; it is the point at which the blue and green lines meet. Here it is estimated that the deglaciation threshold is a mixing ratio of 0.168. Similarly, the glaciation threshold is the point at which the red and green lines meet. This is at a mixing ratio of approximately 0.0004, or 400 ppmv. This is similar to

the present level, but the weaker Neoproterozoic insolation meant that the glaciation threshold was higher than it is today.

We can also determine the effect of convective deepening on the equilibrium phase space of the system[1]. For a mixing ratio of less than 0.01, the dashed and solid lines stay very close, which means that convective deepening alters the situation very little. For mixing ratios greater than that, a few things become apparent. The unstable equilibrium solution is actually warmer than it is without convective deepening. The Snowball solution, on the other hand, is colder. Also, the slopes of both of these lines decrease without convective deepening. Both of these trends together mean that the two lines are far from meeting for a mixing ratio of 0.168, which means that the deglaciation threshold is higher without convective deepening. Indeed, the shallow slopes indicate that, in the absence of convective deepening, the deglaciation threshold would be *significantly* higher.

Including convective deepening narrows the hysteresis loop (i.e., reduces the difference between the glaciation threshold and the deglaciation threshold). This reduces the 'stickiness' of the Snowball state. As Pierrehumbert et al. [19] point out, the stickiness of the Snowball state adds to its explanatory power, but it must not be too sticky to escape; convective deepening helps avoid that conundrum.

8.4 Evolution

We can now infer how the system may have evolved in time during the Neoproterozoic glaciations. The following is a plausible scenario built around Figure 8.6; the exact values are somewhat model-dependent, but give an idea of the system's behaviour.

The pre-glaciation state was on the 'hothouse' branch, with roughly 2000 ppmv of CO_2. The continental breakup then caused an increase in the CO_2 weathering rate, which caused the system to move down the hothouse branch until it reached the glaciation threshold, which is at 400 ppmv. At this point, runaway ice-albedo feedback caused the temperature to drop to 233 K over a timescale of O(1000) years. With most or all of the ocean covered with ice, the CO_2 weathering rate dropped greatly, but the volcanic outgassing continued unabated at a rate of 0.0253 bar per million years. This caused the temperature to steadily rise along the Snowball branch until it reached the deglaciation threshold mixing ratio of 0.168 or 0.3 bar, which took around

[1]Since, per Figure 6.11, pressure broadening never contributes more than 20% of the total warming for this range of p_{I,CO_2}, the difference between the solid and dashed lines is mostly due to convective deepening.

12 million years. At this point, the runaway ice-albedo feedback worked in reverse, ensuring that the planet became ice-free, again in O(1000) years. Because the transition from ice-covered to ice-free is much faster than the CO_2 weathering, the system reaches a new equilibrium while the CO_2 mixing ratio is still 0.168. This equilibrium is a hothouse state, at roughly 350 K. With the entire ocean available once more to interact with the atmosphere, the CO_2 weathering rate now exceeds the outgassing rate and the CO_2 inventory begins to decrease again. Therefore, the peak CO_2 inventory is at the point of deglaciation. From the hothouse equilibrium, the system then moves down the hothouse branch as the CO_2 inventory decreases, until eventually the weathering rate again equals the outgassing rate. At this point, the system is again in a stable equilibrium.

The role of convective deepening in the scenario is to hasten deglaciation; 12 million years is a plausible Snowball duration, while the duration required to accumulate enough CO_2 to deglaciate without convective deepening might exceed the plausible upper limit.

CHAPTER 9

Discussion

The major contribution of this thesis to the literature is the mechanism of convective deepening. This is important both in its own right as a new way to understand the consequences of changing surface pressure, and specifically to the Snowball deglaciation problem as it helps to strengthen a deglaciation scenario consistent with the geological evidence.

The reason we refer to the Snowball deglaciation 'problem' is that the first proposed deglaciation mechanism, a massive CO_2 greenhouse effect, was shown in GCMs to be insufficient to deglaciate the Snowball; further, the logarithmic nature of CO_2 forcing required an implausibly large amount of CO_2 to get a slightly greater warming effect. This led one author to posit that solving the problem would require "as-yet undiscovered processes"[32]; convective deepening is just such a process.

The fast increase of the warming effect due to convective deepening with CO_2 inventory effectively ensures deglaciation for very large inventories, so the notion of a deglaciation scenario requiring more than 1 bar of CO_2 can likely be ruled out.

It is possible that the O_2 partial pressure was around 0.15 bar lower than its present level in the Neoproterozoic [40]. If this was the case, $p_{I,air}$ would be reduced to 0.85 bar. However, adding a given inventory of CO_2 would still give the same *increase* in surface pressure, so, as long as convection still occurred, there would still be convective deepening.

Previously, the main consequence of increasing the surface pressure was thought to be radiative: the broadening of absorption lines. This thesis shows that in many situations there will be a comparable, if not larger,

effect that originates not from the radiative transfer but from the hydrostatic structure of the atmosphere. There are at least two types of situation in which overlooking this effect may be possible.

One is the situation where a model designed for the conditions of the present Earth is used in less familiar conditions, which might cause assumptions, such as the assumption that CO_2 does not contribute to the surface pressure, to break down. This may have been the case for the GCMs used to model the Snowball Earth in early studies.

Another situation is when a parameterisation of radiative forcing as a function of gas inventory (which does not need to be CO_2) may become inadequate if, in the model in question, a change in gas inventory only affects the temperature via its radiative forcing. An example of this is a Budyko-Sellers type energy balance model; an extra increase in surface temperature of O(10) K is surely relevant even to this type of simplified model, so it would be appropriate to include a term representing convective deepening.

Even if a model correctly increases the surface pressure in response to changing gas inventories, it is still valuable to properly categorise the effects in play. For example, without knowledge of convective deepening, one might attribute the warming caused by a surface pressure increase to pressure broadening and conclude that pressure broadening is a more powerful effect than it actually is. With knowledge of neither pressure broadening nor convective deepening, one might conclude that the radiative forcing for a large gas inventory is greater than it actually is.

To ensure the accuracy of atmospheric models when changing atmospheric composition, the work in this thesis supports the approach of calculating the surface pressure as the sum of the inventories of the gases present in the atmosphere. This should make clearer the role that the depth of the troposphere plays in determining the surface temperature. If the surface pressure is calculated in this way, then convective deepening will become an important effect, provided there is a positive surface energy budget to support convection, with the addition of a gas inventory greater than 0.1 bar.

A limitation of this study is the use of a one-dimensional model, which gives only the global average temperature profile. Since the size of the convective deepening warming effect is proportional to the lapse rate, knowledge of the latitudinal distribution of lapse rates would allow convective deepening to be modelled more accurately. This could be investigated with a model consisting of a 1-D radiative-convective model in each latitude band, which accounts for the horizontal heat transfer across each band.

CHAPTER 10

Conclusion

The model achieves deglaciation, which means a global average surface temperature of 263 K, with a CO_2 inventory of 0.25 bar. Without convective deepening the surface is 13.4 K cooler, at 249.6 K, and without pressure broadening it is a further 2.7 K cooler at 246.9 K.

The deglaciation threshold is sensitive to certain model parameters, but convective deepening is shown to be a larger effect than pressure broadening everywhere in the likely deglaciation range of $0.08 - 0.38$ bar, with the suggestion that it also remains the larger effect for thresholds outside this range.

The large CO_2 inventory changes both the specific heat at constant pressure and the specific gas constant of the atmosphere. Accounting for the way this affects the moist adiabatic lapse rate changes the surface temperature by 2.2 K.

This thesis shows that any model that aims to calculate the surface temperature to within 2 K for a large CO_2 inventory (O(0.1 bar) or greater) needs to account for the effect of atmospheric composition on the specific heat at constant pressure and the specific gas constant, and for pressure broadening. Any model that aims for accuracy within 10 K should account for convective deepening.

Bibliography

[1] Nicholas Edkins and Roger Davies. The Effect of Atmospheric Pressure on Snowball Earth Deglaciation. *AIP Conference Proceedings (in press)*, 2016.

[2] Dorian S. Abbot, Aiko Voigt, and Daniel Koll. The Jormungand global climate state and implications for Neoproterozoic glaciations. *Journal of Geophysical Research*, 116(D18103):1–14, 2011.

[3] Christopher P. McKay. Thickness of tropical ice and photosynthesis on a snowball Earth. *Geophysical Research Letters*, 27(14):2153–2156, 2000.

[4] David Pollard and James F. Kasting. Snowball Earth: A thin-ice solution with flowing sea glaciers. *Journal of Geophysical Research C: Oceans*, 110(7):1–16, 2005.

[5] David Pollard and James F. Kasting. Reply to comment by Stephen G. Warren and Richard E. Brandt on Snowball Earth: A thin-ice solution with flowing sea glaciers". *Journal of Geophysical Research*, 111(May):1–7, 2006.

[6] Stephen G. Warren and Richard E. Brandt. Comment on "Snowball Earth: A thin-ice solution with flowing sea glacier" by David Pollard and James F. Kasting. *Journal of Geophysical Research: Oceans*, 111(9):9–11, 2006.

[7] William D. Sellers. A Global Climatic Model Based on the Energy Balance of the Earth-Atmosphere System. *Journal of Applied Meteorology*, 8, 1969.

[8] M. I. Budyko. The effect of solar radiation variations on the climate of the Earth. *Tellus*, 21(5):611–619, 1969.

[9] Joseph L. Kirschvink. Late Proterozoic Low-Latitude Global Glaciation: the Snowball Earth. In *The Proterozoic biosphere: a multidisciplinary study*, pages 51–52. 1992.

[10] K. Caldeira and J. F. Kasting. Susceptibility of the early Earth to irreversible glaciation caused by carbon dioxide clouds. *Nature*, 359:226–228, 1992.

[11] Bernd Bodiselitsch, Christian Koeberl, Sharad Master, and Wolf U. Reimold. Estimating Duration and Intensity of Neoproterozoic Snowball Glaciations from Ir Anomalies. *Science*, 308(5719):239–242, 2005.

[12] P. F. Hoffman, Alan J. Kaufman, Galen P. Halverson, and Daniel P. Schrag. A Neoproterozoic Snowball Earth. *Science*, 281(5381):1342–1346, 1998.

[13] Youxue Zhang and Alan Zindler. Distribution and evolution of carbon and nitrogen in Earth. *Earth and Planetary Science Letters*, 117(3-4):331–345, 1993.

[14] Raymond T. Pierrehumbert. High levels of atmospheric carbon dioxide necessary for the termination of global glaciation. *Nature*, 429(6992):646–649, 2004.

[15] Y. Hu, J. Yang, F. Ding, and W. R. Peltier. Model-dependence of the CO2 threshold for melting the hard Snowball Earth. *Climate of the Past*, 7(1):17–25, 2011.

[16] Dorian S. Abbot, Aiko Voigt, Mark Branson, Raymond T. Pierrehumbert, David Pollard, Guillaume Le Hir, and Daniel D. B. Koll. Clouds and Snowball Earth deglaciation. *Geophysical Research Letters*, 39(20), 2012.

[17] Dorian S. Abbot and Raymond T. Pierrehumbert. Mudball: Surface dust and Snowball Earth deglaciation. *Journal of Geophysical Research: Atmospheres*, 115(3):1–11, 2010.

[18] J. Yang, Y. Hu, and W. R. Peltier. Radiative effects of ozone on the climate of a Snowball Earth. *Climate of the Past*, 8(6):2019–2029, 2012.

[19] R. T. Pierrehumbert, D. S. Abbot, A. Voigt, and D. Koll. Climate of the Neoproterozoic. *Annual Review of Earth and Planetary Sciences*, 39(1):417–460, 2011.

[20] Eli J. Mlawer, Steven J. Taubman, Patrick D. Brown, Michael J. Iacono, and Shepard A. Clough. Radiative transfer for inhomogeneous atmospheres: RRTM, a validated correlated-k model for the longwave. *Journal of Geophysical Research*, 102(D14):16663–16682, 1997.

[21] A. Lacis and V. Oinas. A Description of the Correlated k Distribution Method for Modeling Nongray Gaseous Absorption, Thermal Emission, and Multiple Scattering in Vertically Inhomogeneous Atmospheres. *Journal of Geophysical Research*, 96(D5):9027–9063, 1991.

[22] Andrew A. Lacis and James E. Hansen. A Parameterization for the Absorption of Solar Radiation in the Earth's Atmosphere. *Journal of the Atmospheric Sciences*, 31(1):118–133, 1974.

[23] Syukuro Manabe and Robert F. Strickler. Thermal Equilibrium of the Atmosphere with a Convective Adjustment. *Journal of the Atmospheric Sciences*, 21(4):361–385, 1964.

[24] Graeme L. Stephens and Tristan L'Ecuyer. The Earth's energy balance. *Atmospheric Research*, 166:195–203, 2015.

[25] Syukuro Manabe and Richard T. Wetherald. Thermal Equilibrium of the Atmosphere with a Given Distribution of Relative Humidity. *Journal of the Atmospheric Sciences*, 24(3):241–259, 1967.

[26] David Andrews. *An Introduction to Atmospheric Physics*. 2010.

[27] B. Hassler, G. E. Bodeker, I. Cionni, and M. Dameris. A vertically resolved, monthly mean, ozone database from 1979 to 2100 for constraining global climate model simulations. *International Journal of Remote Sensing*, 30(15-16):4009–4018, 2009.

[28] Douglas Mason. Mean Tropospheric Lapse Rate and a One Dimensional Radiative Convective Climate Model (unpublished dissertation). 2011.

[29] National Oceanic Administration and Atmospheric. U.S. Standard Atmosphere, 1976.

[30] Dorian S. Abbot. Resolved Snowball Earth Clouds. *Journal of Climate*, 27(12):4391–4402, 2014.

[31] Claudio Tomasi, Alessandra Cacciari, Vito Vitale, Angelo Lupi, Christian Lanconelli, Andrea Pellegrini, and Paolo Grigioni. Mean vertical profiles of temperature and absolute humidity from a 12-year radiosounding data set at Terra Nova Bay (Antarctica). *Atmospheric Research*, 71(3):139–169, 2004.

[32] R. T. Pierrehumbert. Climate dynamics of a hard snowball Earth. *Journal of Geophysical Research D: Atmospheres*, 110(1):1–22, 2005.

[33] Dennis L. Hartmann and Kristin Larson. An important constraint on tropical cloud-climate feedback. *Geophysical Research Letters*, 29(20):1951:12, 2002.

[34] Guillaume Le Hir, Yannick Donnadieu, Gerhard Krinner, and Gilles Ramstein. Toward the snowball earth deglaciation... *Climate Dynamics*, 35(2):285–297, 2010.

[35] Guillaume Le Hir, Yannick Donnadieu, Gerhard Krinner, and Gilles Ramstein. Toward the snowball earth deglaciation... *Climate Dynamics*, 35(2):285–297, 2010.

[36] Guillaume Le Hir, Gilles Ramstein, Yannick Donnadieu, and Raymond T. Pierrehumbert. Investigating plausible mechanisms to trigger a deglaciation from a hard snowball Earth. *Comptes Rendus - Geoscience*, 339:274–287, 2007.

[37] J. P. Lewis, a. J. Weaver, and M. Eby. Deglaciating the snowball earth: Sensitivity to surface albedo. *Geophysical Research Letters*, 33(23):1–5, 2006.

[38] Thomas J. Crowley, William T. Hyde, and W. Richard Peltier. CO2 levels required for deglaciation of a nearsnowball Earth. *Geophysical Research Letters*, 28(2):283, 2001.

[39] Raymond T. Pierrehumbert. *Principles of Planetary Climate*. 2009.

[40] Don E. Canfield, Simon W. Poulton, and Guy M. Narbonne. Late-Neoproterozoic Deep-Ocean Oxygenation and the Rise of Animal Life. *Science*, 315(5808):92–95, 2007.